MLM-2241

MLM-2241

Mound Laboratory Activities for the Division of Physical Research: January-June 1975

November 11, 1975

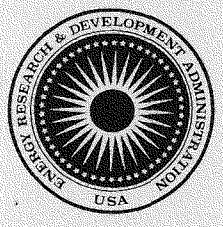

Research and Development Report

MOUND LABORATORY
Miamisburg, Ohio
operated by
MONSANTO RESEARCH CORPORATION
a subsidiary of Monsanto Company
for the
UNITED STATES ENERGY RESEARCH AND DEVELOPMENT ADMINISTRATION

U. S. Government Contract No. E-33-1-GEN-53

Monsanto

MLM-2241
TID-4500
Distribution Categories UC-4 and 22

Mound Laboratory Activities for the Division of Physical Research: January-June 1975

Issued: November 11, 1975

Available from
National Technical Information Service
U. S. Department of Commerce
5285 Port Royal Road
Springfield, Virginia 22161
Price: Printed Copy $5.45; Microfiche $2.25

MONSANTO RESEARCH CORPORATION
A Subsidiary of Monsanto Company

MOUND LABORATORY
Miamisburg, Ohio 45342
operated for

UNITED STATES ENERGY RESEARCH AND DEVELOPMENT ADMINISTRATION

U.S. Government Contract No. E-33-1-GEN-53

NOTICE
This report was prepared as an account of work sponsored by the United States Government. Neither the United States nor the United States Energy Research and Development Administration, nor any of their employees, nor any of their contractors, subcontractors, or their employees, makes any warranty, express or implied, or assumes any legal liability or responsibility for the accuracy, completeness or usefulness of any information, apparatus, product or process disclosed, or represents that its use would not infringe privately owned rights.

Foreword

The Mound Laboratory Activities for the Division of Physical Research report, issued semiannually, replaces the previously published quarterly reports, Stable Gaseous Isotope Separation and Purification and the Mound Laboratory Chemistry and Physics Progress Report. Under the sponsorship of the ERDA Division of Physical Research, Mound is responsible for furnishing material to be used in the physical sciences to further the progress of science and technology in the public interest. Additional research activities of related interest under the sponsorship of the Division of Military Applications are also published in this report.

This report is submitted by W. T. Cave, Director of Nuclear Operations, and R. E. Vallee, Manager of Technology Applications and Development, from contributions prepared by W. M. Rutherford, Science Fellow (Thermal Diffusion); W. L. Taylor, Science Fellow (Gas Dynamics and Cryogenics); G. L. Silver, Senior Research Specialist (Separation Chemistry); R. J. De Sando, Advanced Development Manager; and from members of the Isotope Separation Section: R. A. Schwind, Isotope Separation Manager; E. Michaels, Leader, Isotope Separations Development; W. J. Roos, Leader, Stable Isotopes Production; B. E. Jepson, Leader, Metal Isotope Separation; R. M. Watrous, Leader, Radioisotopes Separation; and V. L. Avona, Leader, Stable Isotope Sales.

These reports are not intended to constitute publication in any sense of the word. Final results will either be submitted for publication in regular professional journals or be published in the form of MLM topical reports.

R. E. Fitzharris, Editor

Table of Contents

Computer Installation

COMPUTER INSTALLATION IN HH-BUILDING

Plans have been completed for the acquisition of a "stand-alone" computer system in HH-Building. The first phase of this installation should be completed by the end of June. This report identifies those areas which will benefit most directly from computer support and describes the hardware/software system chosen to satisfy the needs of those areas.

I. Areas of Computer Application

Some of the areas that will benefit by having access to a computer system are listed in Table 1. These areas cut across all programs which are performed in HH-Building including 1) the production of stable isotopes for commercial use, 2) applied research in the areas of gaseous and liquid isotope separations, and 3) basic research into the transport properties of gases and liquids.

Instrument Control and Data Acquisition

Plans for instrument control include 1) a CEC "620" cycloidal mass spectrometer which will be used for process control analyses from the various isotope separation processes, 2) an electric-quadrupole mass spectrometer which will be used for analyses, both in the areas of production and applied research, and 3) a second quadrupole mass spectrometer which is currently being installed as the primary detector in a beam scattering chamber and will be used in the measurement of cross sections. In the future we foresee the need for another research-grade mass spectrometer, possibly used in conjunction with gas chromatographic equipment.

Each of the instruments listed above is capable of delivering a large quantity of information which can be handled most effectively by instituting some means of automation. This capability is particularly important in the area of process monitoring where accurate results must be quickly available for control purposes.

Table 1

AREAS OF COMPUTER APPLICATION FOR THE ISOTOPE SEPARATION FACILITY

I. Instrument Control and Data Acquisition (Real-Time)
   - A. CEC "620" cycloidal mass spectrometer
   - B. Extranuclear quadrupole mass spectrometer
   - C. Extranuclear quadrupole mass spectrometer used as a detector for the beam scattering chamber

II. Data Reduction
   - A. Real-time, during data acquisition
   - B. Off-line, via interactive terminal
   - C. Off-line, via "batch" mode

III. Process Monitoring and Control
   - A. Ne thermal diffusion
   - B. Kr thermal diffusion
   - C. Sulfur chemical exchange (new system)
   - D. Calcium chemical exchange (proposed system)

IV. General Computations
   - A. Process modeling (for example, cascade theory)
   - B. Quantum mechanical calculations for transport phenomena
   - C. Salable item inventories

Data Reduction Data reduction can be accomplished in several ways. Data from the mass spectrometers can be accurately and efficiently reduced with the aid of a computer, which is necessary for the results to be usable in process control. Additionally, end-product analyses must be accurate since isotopes are sold on the basis of their isotope ratios and impurity levels.

Process Monitoring and Control In the area of isotope separation (both research and production facilities), there are a large number of parameters (for example, temperature, pressure, flow rate) which must be monitored on a routine basis in order to initiate the correct control responses. At present, these control responses are manual operations. On this basis, manpower must be increased to keep pace with the number and complexity of systems. This is not only wasteful of manpower but also increases the chance for error, which in certain processes can be quite costly.

Once the capability for process automation has been established, new systems can be added with a minimum of effort and with minimum increases in manpower for monitoring and control purposes.

General Computations There are computational programs of a general nature which would be of increased utility provided they could be run with quick turnaround times. This is particularly true with certain process modeling codes which must be run several times while varying the input parameters. Large computational programs will continue to be run on the IBM 360/55. If the time does come where it is necessary to set up a data link with the IBM 360, this can be accomplished with the existing hardware and software available for MODCOMP.

II. Computer System Description

It can be seen from the above needs that the proposed system must be more than a dedicated process controller. There are a wide variety of automated tasks to be performed, many of which must be performed simultaneously. For example, mass spectroscopic gas analyses must proceed throughout working hours whenever they are needed. Concurrently and independently, scattering chamber control and data acquisition tasks might be required. Still further, program development and debugging functions must be carried out. It is impractical to require use of the full system in order to perform any of these functions exclusively.

A practical solution for the minimization of necessary hardware is to operate with a computer system capable of supporting a multiprogramming environment.

II. A. System Hardware: MODCOMP IV

The system to be installed is a MODCOMP IV (Modular Computer Systems, Ft. Lauderdale, Fla.). The system is to be delivered and placed in operation by the end of July 1975. Figure 1 shows the overall hardware configuration that will be installed initially.

The MODCOMP design goal was to produce a system capable of effective operation in a multiprogramming, multiprocessor environment. Thus, the computer has features which greatly reduce both software and time overhead associated with multitask operations. For example, the MODCOMP IV uses a four-port memory controller which allows the CPU, I/O bus, a second high-speed I/O bus, and an external processor to have unique access paths. This, in turn, allows multiple memory transfers within the same memory cycle time. The effective memory cycle time is 500 nsec (16-bit). The microprogrammed instruction set provides for bit, byte, word (16-bit) and double word (32-bit) arithmetic and logic operations. The floating point processor handles up to 64-bit floating point numbers. There are 16 general-purpose registers and a context file composed of 16 sets (15 registers per set) of registers. Each executing program is assigned one of these files for its own use. When the currently executing program causes a change in one of the working registers, the corresponding register in its assigned context file is changed simultaneously. This "tracking" frees the system from the necessity of saving registers when the program is interrupted. During the context switching time, before the highest priority program begins execution, its assigned context file is transferred to the working register file at virtually no overhead to the program. This technique results in a context switching time of 3 μsec as opposed to the usual 100-150 μsec.

The multiprogramming environment is also enhanced by the Memory Management System which includes four memory mapping files. These files allow up to seven programs to

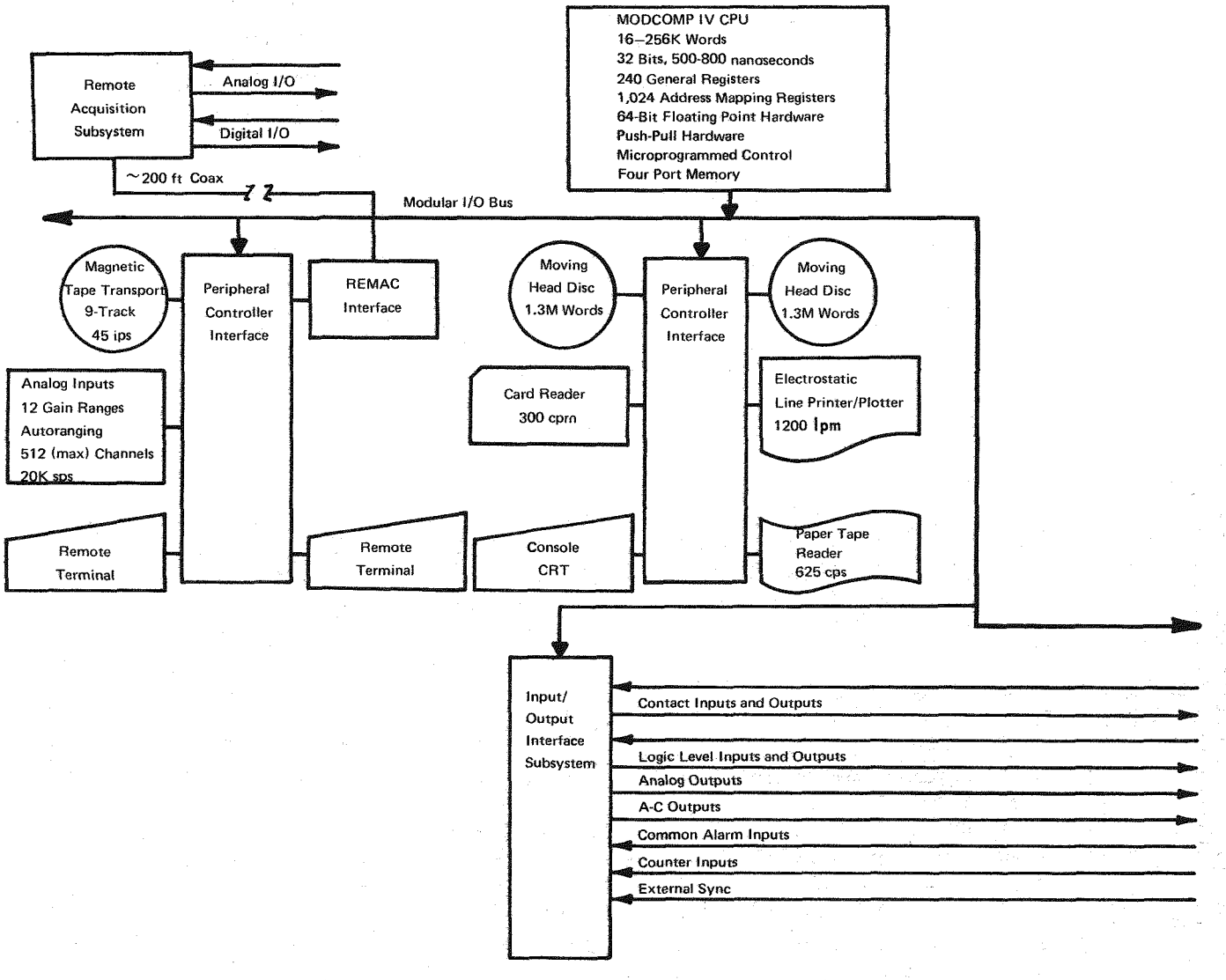

FIGURE 1 - MODCOMP IV hardware.

be mapped at any given time. The computer can operate in a "virtual" memory mode where the 16-bit effective address referenced in an instruction is transformed, through the tasks map file, to an 18-bit physical address. This mapping is done on a page (256 word) basis and results in complete protection between operating programs in memory.

The addressing space of each program begins at virtual address "o" which constitutes a form of absolute addressing. Thus, programs are loaded into memory at direct memory access speeds. No hardware relocation is necessary. All address translation is done by the Memory Management System at instruction execution time. Both register and direct memory access I/O transfers are implemented with priority vectored interrupt capability available separately for data and service requests from each device.

In the future, several remote process control/data acquisition stations are planned. The first remote station to be developed, as indicated in Figure 1, will be for control and data acquisition functions associated with the beam scattering chamber in HH-Building. For this application, a Remote Acquisition Subsystem will be installed. This subsystem, manufactured by MODCOMP, is designed for remote operation up to 10,000 ft, supports both analog and digital I/O, and interfaces to the MODCOMP IV via a single coaxial cable. I/O functions are implemented by the use of plug-in cards.

In applications that require large, continuous, I/O transfer rates, it will be advantageous to use mini (micro) computers as local controllers. For these situations, the MODCOMP IV will be used in a supervisory capacity. Various microprocessor alternatives are being studied.

II. B. System Software: MAX IV

The MAX IV software system is a multiprogramming executive that accommodates concurrent execution of real-time, interactive, and batch-type programs. Software priority is assigned to each executing program. Time is allocated to batch operations when real-time programs are waiting on I/O, timers, etc.

It is planned that all programs, including real-time programs, will be coded in FORTRAN. MODCOMP supplies a FORTRAN compiler which incorporates the real-time extensions adopted by the Purdue Workshop. In-line machine language coding is permitted by the compiler when specialized situations demand it.

Also, a BASIC compiler is supplied by MODCOMP and will be available if it becomes advantageous to use that language at some future time.

III. Immediate Objectives

At first, the programming emphasis will be divided between developing real-time data acquisition programs and in converting existing FORTRAN programs to run under the batch subsystem.

The first real-time FORTRAN programs to be developed will be for data acquisition and reduction from the "620" cycloidal mass spectrometer. This is the primary instrument used for process control analyses. Work is already in progress towards the development of these programs. These programs will also be useful, at least in part, for operation of the two quadrupole mass spectrometers currently being used in HH-Building.

Another area of effort is that of modifying existing FORTRAN programs to run on the MODCOMP IV. The first project is one of adapting cascade theory programs. These programs are very useful in predicting column behavior and must be run frequently for a variety of cases. Also, work is currently in progress on the design of a program for product inventory control. We hope to have these programs in operation by this fall. Other projects will be developed concurrently at a slower pace. In particular, plans are being made for various process monitoring and control functions. *(R. E. Eppley)*

Isotope Separation

ARGON

During this period, the 13-column hot wire thermal diffusion cascade was restarted for the production of argon-36 and intermediate argon-38. The configuration of this cascade, from the top down, is 1-1-1-2-8. Natural abundance argon is being circulated across the bottom of the system, and argon-36 is being produced at the top at greater than or equal to 99.5%. Argon-38 will be withdrawn from the bottom of the second stage when its concentration reaches approximately 25%. This material will be collected and stored until there is a sufficient quantity to fill a system for further enrichment greater than or equal to 95%. *(G. E. Stuber)*

CARBON

During this period, a 130-STP liter batch of methane with a carbon-13 concentration greater than 97% was produced by thermal diffusion. Also produced by thermal diffusion were three batches of methane, totaling 340 STP liters, with carbon-13 concentrations greater than 99%. The feed materials used for these enrichments had carbon-13 concentrations in the 80-90% range. *(W. J. Roos)*

KRYPTON

A 19-column thermal diffusion cascade has been modified by moving the product draw-off down one stage from the top. This modification has resulted in a change in the product concentration from 90% to 50% krypton-78, and the production rate at this new concentration has been increased from 23 ml/day to 48 ml/day. The top stage was left open to the system and is used to collect and remove contaminants. This top stage is also building a krypton-78 inventory for subsequent production of 99% krypton-78. The failure of an electrical contactor during this period resulted in the loss of about two weeks of production time.

The nine-column, five-stage thermal diffusion cascade has continued to produce krypton intermediate for subsequent enrichment of krypton-82 and krypton-83. The concentration of these desired isotopes (krypton-82 and krypton-83) has been increased by making minor adjustments to the flow rates in the top and bottom streams.

The 19-column, seven-stage thermal diffusion cascade has continued to produce feed material for the cascade enriching krypton-83. This cascade has also produced krypton-82 and -80. Minor adjustments in the bottom flow rate have improved the recovery of krypton-83.

The 10-column, nine-stage cascade, which is used to enrich krypton-83, developed a leak during this period, resulting in a loss of most of the inventory of krypton-83 in the system. Sufficient feed material was available to refill the system, which is presently rebuilding a productive concentration profile. *(G. E. Stuber)*

Radiometric Krypton The goal of this program is to produce a quantity of krypton which is highly depleted in krypton-85. During this period, processing of the second batch was completed, and the material was shipped. Processing of the third batch is currently underway. *(W. J. Roos)*

NEON

Production of neon-21 at greater than or equal to 90% has continued in two experimental systems. The two cascades are connected in series so that the first cascade produces a binary neon mixture of neon-21 and neon-22 which is highly depleted in neon-20. This material is then fed to the second cascade which strips the neon-22 from the product. *(G. E. Stuber)*

XENON

During this period, a 24-column thermal diffusion system produced 1.23 STP liters of 20% xenon-124. This system had been modified earlier in the current fiscal year, and the production rate achieved since modification is approximately 50%

greater than had been attained in the past. A 19-column thermal diffusion system produced 0.83 STP liter of 40% xenon-124.

An eight-column hot wire thermal diffusion system produced 0.47 STP liter of 99% xenon-136, 0.42 STP liter of 90% xenon-136, 2.53 STP liters of 80% xenon-136, and 0.7 STP liter of 60% xenon-131 during the period. *(W. J. Roos)*

Low Temperature Research

VAPOR PRESSURE STUDIES

The work during this period has been divided into four areas: 1) a review of the properties of superfluid ^3He is in process as a topical report (MLM-2202), 2) seven liters of e-D_2 were prepared in the cryostat described in the last report[1] for the ortho-para D_2 vapor pressure measurements; however, several successive electronic failures have delayed the measurements several months, 3) a cryostat has been designed and is being fabricated for use in a SW tritium laboratory where two experiments are planned, namely, a study of the inverse isotope effect of superconductivity in PdX (X being H_2, D_2, or T_2) and a determination of the low temperature phase diagram of D_2-T_2 from vapor pressure measurements, and 4) a second cryostat is being designed for differential calorimetry of liquid and solid mixtures of isotopes available at Mound.

The topical report on the superfluid properties of ^3He was an outgrowth of a seminar given at Mound Laboratory on a portion of a NATO International Summer School on Quantum Solids and Fluids. The treatment of the subject in the report will be on a level understandable to those not involved in superfluid research.

In making the e-D_2, about 10 cc of liquid normal D_2 was condensed in the presence of the chrome-alumina catalyst. The freezing and melting of the D_2 at a pressure of 128 mm of mercury was visually apparent. The sample was held at one atmosphere pressure (approximately 23 K) for 8 hr and then expanded into the 5 liter glass storage bulb. Two such batches of e-D_2 were made. The difference in thermal conductivity of the e-D_2 and n-D_2 was measured using the matched Pirani gauges in a conductivity bridge. The two e-D_2 samples each produced a 19 mV off balance compared to n-D_2 with a repeatability of about ±0.5 mV. Thus, the percentage of ortho species can be determined to about ±0.8%. The presence of HD in the D_2 has been reduced to less than 1%. The vapor ratio experiments were set to begin but were delayed by a series of electronic failures in the Baratron, thermometer power supply, and detector. Repairs have been effected, and the experiments have been restarted.

In the meantime, two new cryostats have been designed and one is being fabricated. The one being fabricated will be used for tritium experiments in SW-Building. Two inserts for the cryostat are being made. One is a differential vapor pressure bulb which will be used to determine the low temperature phase diagram for D_2-DT-T_2. Precise measurements will be made against a D_2 vapor pressure standard. The second low temperature cell being constructed will measure the superconducting transition temperature in PdT_x compounds to study the inverse isotope effect in PdH, PdD, and PdT. Measurements on PdH_x and PdD_x have been made in several laboratories. Mound will make the PdT_x measurements. A diagram of the measuring apparatus is shown in Figure 2. Pd powder is put in the end of a high pressure tube and reacted with tritium gas up to several hundred bars to provide PdT_x for different values of x. Then the sample is cooled and the excess T_2 gas pumped off. As the sample is cooled to 1 K, the superconducting transition is shown by a change in mutual conductance. It is expected that a value of x corresponding to 1 atm T_2 at 300 K will produce a transition at about 2 K; whereas a value of x=1, which corresponds to PdT, will produce a transition temperature at about 14 K or 15 K. The actual transition temperature values will help to determine which of several models of the inverse isotope effect is correct.

The second cryostat is being designed to measure heat capacities of liquified and solidified mixtures of permanent gases. The mixtures will be measured differentially against a pure sample. The excess heat capacity of the mixture is a direct measure of clustering of like molecules. A new theory, taking into account optimum clustering, relates the clustering to the intermolecular potential between unlike atoms. The design of the calorimeter will allow condensing and freezing of samples of the order of 1 mole in size using a mechanical heat switch to cool samples to the order of 1 K, and it is planned to feed the data from the calorimeter into the HH-Building computer system. *(G. T. McConville)*

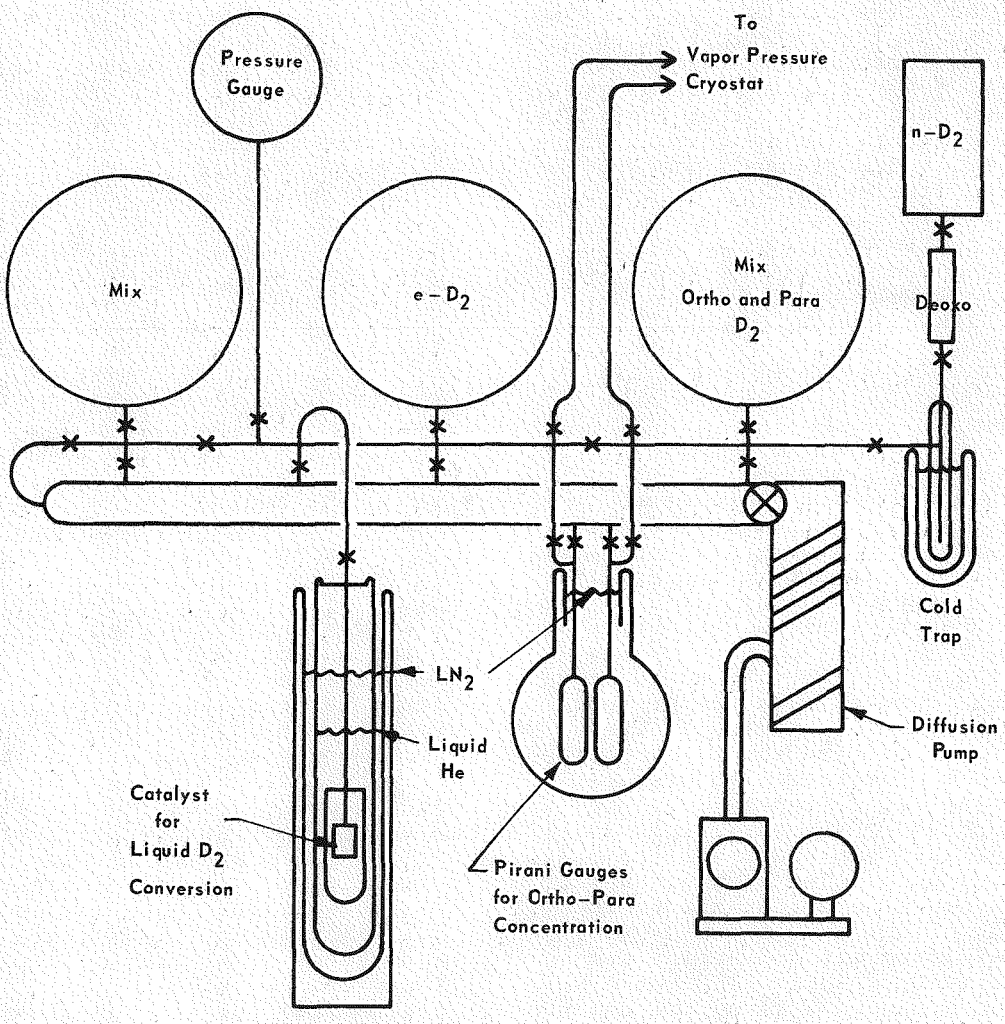

FIGURE 2 - Storage and conversion system for ortho-para D mixtures.

Metal Hydride Research

APPLICATION OF STATISTICAL MECHANICS

We are now writing a review article on important statistical mechanical models that have been developed to explain the thermodynamic behavior of non-ionic metal hydrides. These models are discussed in terms of their relationship to a more general, relatively rigorous statistical representation of metal hydrides. In this way, we hope to gain a clear understanding of the approximations involved in existing models.

We also show the analog of these models to statistical mechanical representations of other important systems, such as real gases and binary alloys. The elucidation of these analogies has provided some important insights into the behavior of metal hydrides.

A discussion of the importance of elastic interactions, with special emphasis on their role in Group V hydrides, has been included in this review. This is a recent development that has provided valuable insight into the nature of interactions between interstitially bound species.

The overall purpose of this review is to provide a framework that will guide future development of more realistic statistical models to represent not only simple metal hydrides, but alloy hydrides as well.
(G. C. Abell)

BAND THEORY CALCULATIONS

There have been four stages in the development and use of the self-consistent plane wave Gaussian (SCPWG) computer codes:

1. Major revision of the computer codes so that properties of metals could be calculated.

2. Feasibility studies to determine the computer resources necessary for crystals with such relatively large atoms as Pd.

3. Calibration of the computer codes against previous results for simple systems and against accurate Hartree-Fock crystalline results for Li and LiH.

4. Production runs for the transition metal hydrides of interest.

Stages 1 and 2 were completed within the first six months of the current year. The major accomplishments of the last six months have been the attainment of Stage 3 for Li and LiH and Stage 4 for a representative system NiH. From the electronic charge density $\rho(\vec{r})$ and the one-electron energies, one can calculate the total energy per unit cell for a crystal. Figures 3 and 4 show this quantity for several values of the lattice constant for Li. Figure 5 gives the Hartree-Fock results for Li. Figures 6 and 7 show the total energy per unit cell for several values of the lattice constant for LiH. The value of α in Figures 3, 4, 6, and 7 is the so-called exchange constant by which one uses the local-density exchange approximation (LDEA) to approximate the true Hartree-Fock exchange. Figure 8 gives the Hartree-Fock results for LiH.

The calculated lattice constant, bulk modulus (or its reciprocal, compressibility), and lattice energy can be determined by fitting an analytic function to the calculated points. These quantities are presented in Tables 2 and 3 for Li and LiH, respectively. These results clearly show the major limitation of the LDEA, namely, all the values are strongly dependent upon the exchange constant α. To this date, there is no logical prescription for choosing a value of α for crystals with more than one atom type per unit cell. However, there are two possible approaches to this problem. First, one can attempt to modify the present model of the LDEA by choosing various values of α in different regions of the crystal. This approach is not very appealing because there is no sound physical basis for it and because it is difficult to apply for most computer codes which do not use the muffin-tin

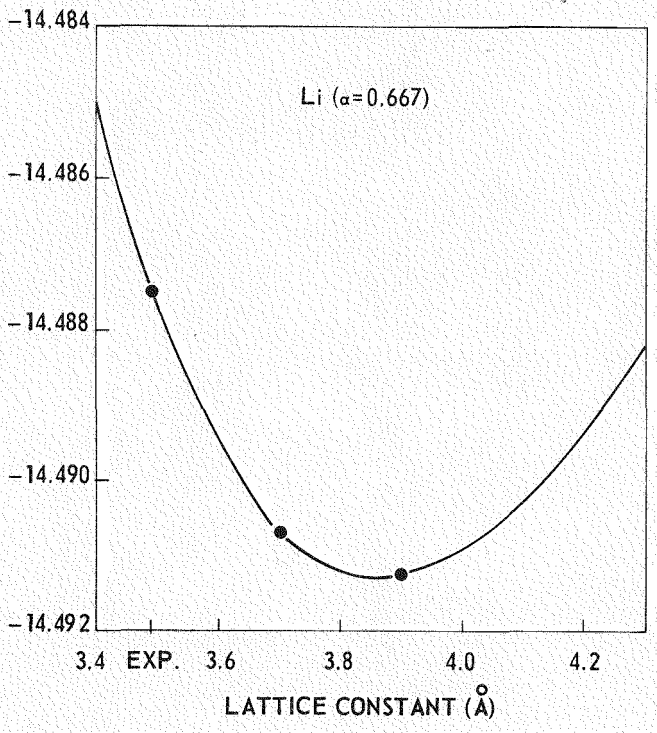

FIGURE 3 - Total energy per unit cell for several values of the lattice constant for Li.

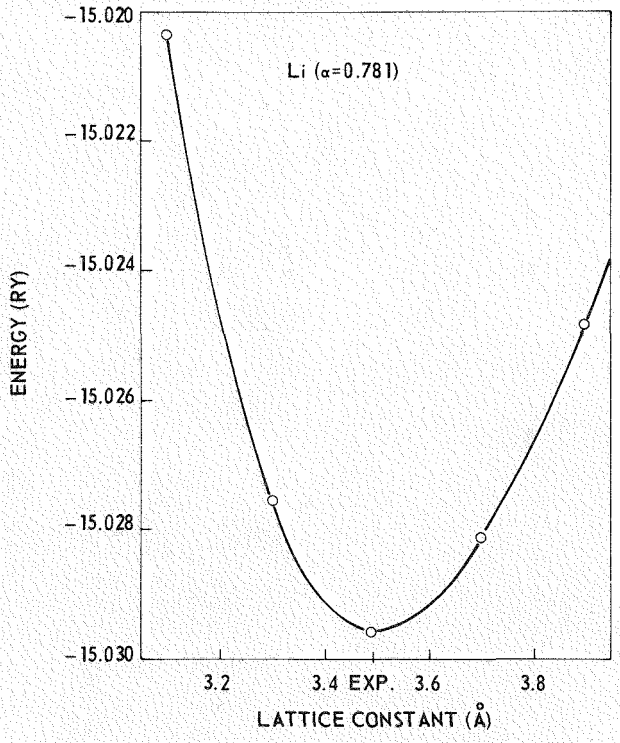

FIGURE 4 - Total energy per unit cell for several values of the lattice constant for Li.

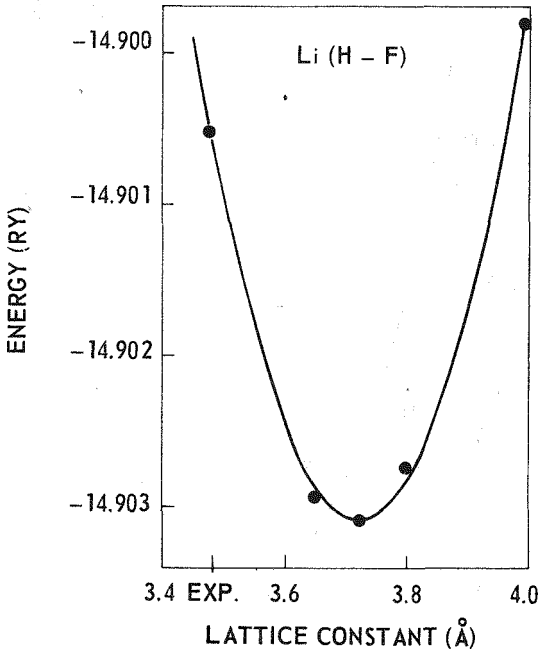

FIGURE 5 - Hartree-Fock results for Li.

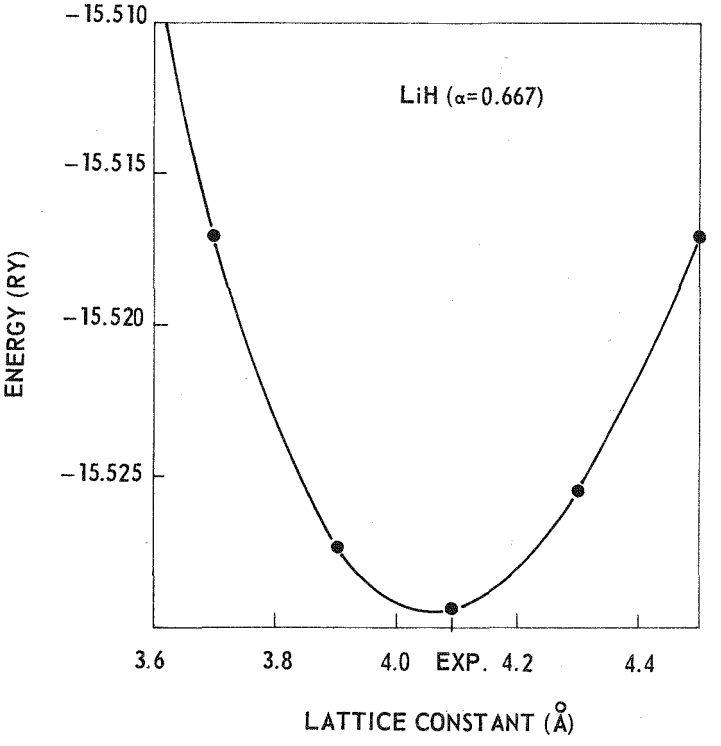

FIGURE 6 - Total energy per unit cell for several values of the lattice constant for LiH.

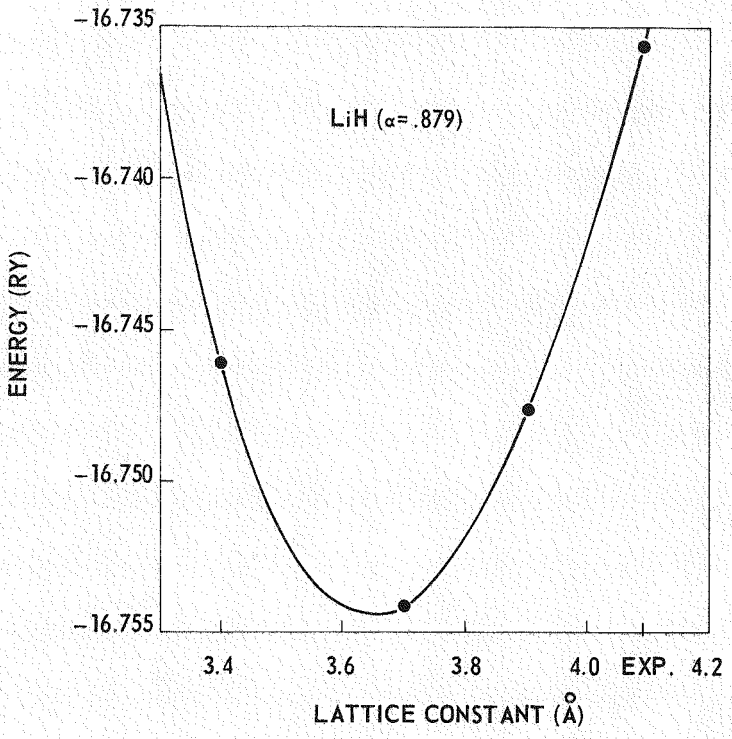

FIGURE 7 - Total energy per unit cell for several values of the lattice constant for LiH.

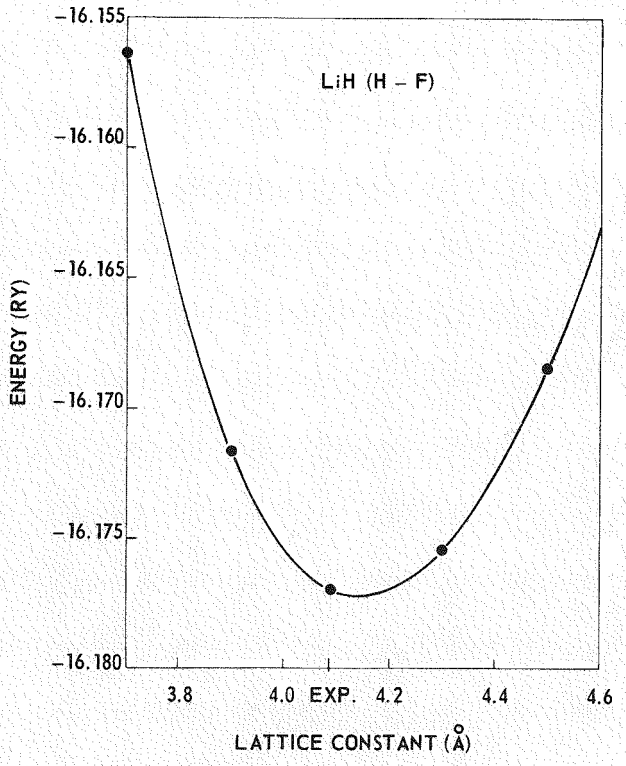

FIGURE 8 - Hartree-Fock results for LiH.

Table 2

GROUND-STATE PROPERTIES OF LITHIUM

	Exp.	H-F	α=0.667	α=0.781
a_L	3.491Å	3.707Å	3.859Å	3.501Å
E_C	1.65eV	0.51eV	1.93eV	2.27eV
B[a]	0.121	0.116	0.053	0.112

[a] B is in units of 10^{12} dynes/cm^2.

Table 3

GROUND-STATE PROPERTIES OF LITHIUM HYDRIDE

	Exp.	H-F	α=0.667	α=0.880
a_L	4.083Å	4.145Å	4.060Å	3.644Å
E_C	4.81eV	4.25eV	4.92eV	6.83eV
B[a]	0.347	0.392	0.380	0.643

[a] B is in units of 10^{12} dynes/cm^2.

potential approximation. Second, one can reformulate the idea of a local approximation to the Hartree-Fock exchange that does not utilize any electron gas model (as does the LDEA in its present formulation). Work is continuing in this latter area to develop more accurate ideas of approximating the Hartree-Fock exchange.

Preliminary results have been obtained for NiO and NiH within the LDEA. These two crystalline systems are being studied to observe the difference in the Ni charge density between them. Computer codes are now being developed to display graphically in two- and three-dimensions the electronic charge density. The SCPWG computer programs will be slightly modified so that only the bonding charge density will be displayed and not the core charge density.

The most important part of the FY-75 activities has been the continued development of the SCPWG computer programs. For this reason, a continuing effort is being made to improve the accuracy and to decrease the computer time necessary to run a given system. Within the last six months, major changes have been implemented in the codes which have resulted in increased accuracy for larger systems and a central processor (CPU) time savings of 20-25% at no cost in computer memory or any other resource. The ideas involved in these changes suggest other possible changes which should also result in significant CPU time savings.

The SCPWG programs require an extremely large data file for storage of intermediate data. In the self-consistent cycle, there is a large amount of peripheral processor (PP) time involved in reading this file. The changes in computer coding necessary to convert this file from a sequential file to a random access file have been worked out. All that remains is the implementation of these changes and the subsequent testing of the new package. It is expected that these changes could result in a 25-50% decrease in PP time which is just as real a cost as CPU time. *(J. L. Ivey)*

PULSE NMR STUDIES

During the first year of the metal hydride project, the emphasis of the nuclear magnetic resonance (NMR) studies has been on developing and evaluating various pulse

techniques. In particular, the capabilities of present equipment for investigating metal hydrides has been determined; and the analysis methods have been applied to suitable examples.

Diffusion Studies in VH_x NMR studies of the vanadium-hydrogen system are of interest for several reasons. First, three distinct phases (that is, bcc, bct, and fcc) are formed depending upon the hydrogen concentration and temperature. The locations of the hydrogen atoms among several possible interstitial sites are still unsettled for these phases. Local ordering of hydrogen atoms occurs at low temperatures (that is, <200 K). Finally, vanadium dihydride has excellent characteristics for hydrogen storage material.

The initial NMR measurements were performed on a sample of $VH_{0.53}$ prepared at Mound Laboratory by R. S. Carlson. X-ray diffraction indicated this material possessed a body-centered tetragonal (bct) crystal structure with lattice parameters a_o = 3.001 ±0.003 Å and c_o = 3.311 ±0.004 Å. These results agreed with the previous data obtained by Maeland[2] for β-phase VH_x. The diffusion behavior of protons in VH_x was investigated by measuring the temperature dependence of the spin-lattice relaxation time (T_1) using a three pulse sequence.

The T_1 data for $VH_{0.53}$ are shown in Figures 9 and 10. The influences of both temperature and proton resonance frequency have been observed. The minima in these figures indicate the major relaxation mechanism is thermally-activated proton diffusion. A break in the T_1 temperature dependence is observed at high temperatures. This behavior is consistent with the phase transition[2] from β to α-phase (that is, bcc) which occurs at ~450 K. The proton mobility in the α-phase is so rapid at these temperatures that the main contribution to T_1 arises from interactions with conduction electrons. Consequently, the current interest is centered on determining proton diffusion in the β-phase from the T_1 data.

The determination of the proton self-diffusion requires that the T_1 data be analyzed in terms of the correlation time τ_c, where τ_c is the mean time a proton spends at a stable lattice site before jumping to a neighboring site. If the diffusion process for a powder sample of high symmetry material can be described by an exponential correlation function with a single correlation time, the dipolar spin-lattice relaxation time T_{1d} is related to τ_c by the expression:

$$(T_{1d})^{-1} = \frac{2}{5} C_I \left\{ F(\omega_I) + 4F(\omega_I) \right\} \sum_i (r_i^{-6}) + \frac{2}{5} C_S \left\{ \tfrac{1}{3} F(\omega_I - \omega_S) + F(\omega_I) + 2F(\omega_I + \omega_S) \right\} \sum_j (r_j^{-6}), \quad (1)$$

where

$$F(\omega) = \frac{\tau_c}{1 + \omega^2 \tau_c^2} . \quad (2)$$

Here, $C_I = \gamma_I^4 \hbar^2 I (I + 1)$,

$C_S = \gamma_I^2 \gamma_S^2 \hbar^2 S (S + 1)$, $\omega_I = \gamma_I H_o$,

$\omega_S = \gamma_S H_o$, γ_I and γ_S are the gyromagnetic ratios of spins I and S respectively, H_o is the magnetic field strength, $\hbar$ is Planck's constant divided by 2π, and I and S apply to hydrogen and metal nuclei, respectively. The summations $\sum_i (r_i^{-6})$ and $\sum_j (r_j^{-6})$ refer to sums over hydrogen and metal sites respectively with the origin at a hydrogen site. Eq. (1) assumes that only one type of hydrogen lattice site is occupied. The hydrogen diffusion is also assumed to be uncorrelated and nuclear quadrupole effects for the metal (that is, Group V) nucleus are neglected. This expression is known as the BPP model and has been extensively used to study[3] diffusion in metal hydrides.

The application of Eq. (1) and (2) to the T_1 data in Figures 9 and 10 requires that the distribution of hydrogen atoms in VH_x be known. Although the hydrogen sites have not been firmly established,[4] recent studies[5,6] indicate the protons are randomly distributed on the pseudo-octahedral sites which lie along the c_o axis between the vanadium atoms. This hydrogen location is responsible for the tetragonal elongation of the bcc vanadium lattice. The lattice sums in Eq. (1) have been directly calculated in the present study for this hydrogen distribution and are:

$$\sum_i (r_i^{-6}) = 24.51\ a_o^{-6}$$

$$\sum_j (r_j^{-6}) = 110.20\ a_o^{-6},$$

where the c_o/a_o ratio is 1.103. Substitution of these lattice sums into Eq. (1) and and evaluation of the other parameters indicates the vanadium-proton dipolar interaction is ~12 times larger than the proton-proton dipolar interaction for T_{1d}. Hence, the evaluation of τ_c can be determined to a good approximation using only the vanadium-proton term as:

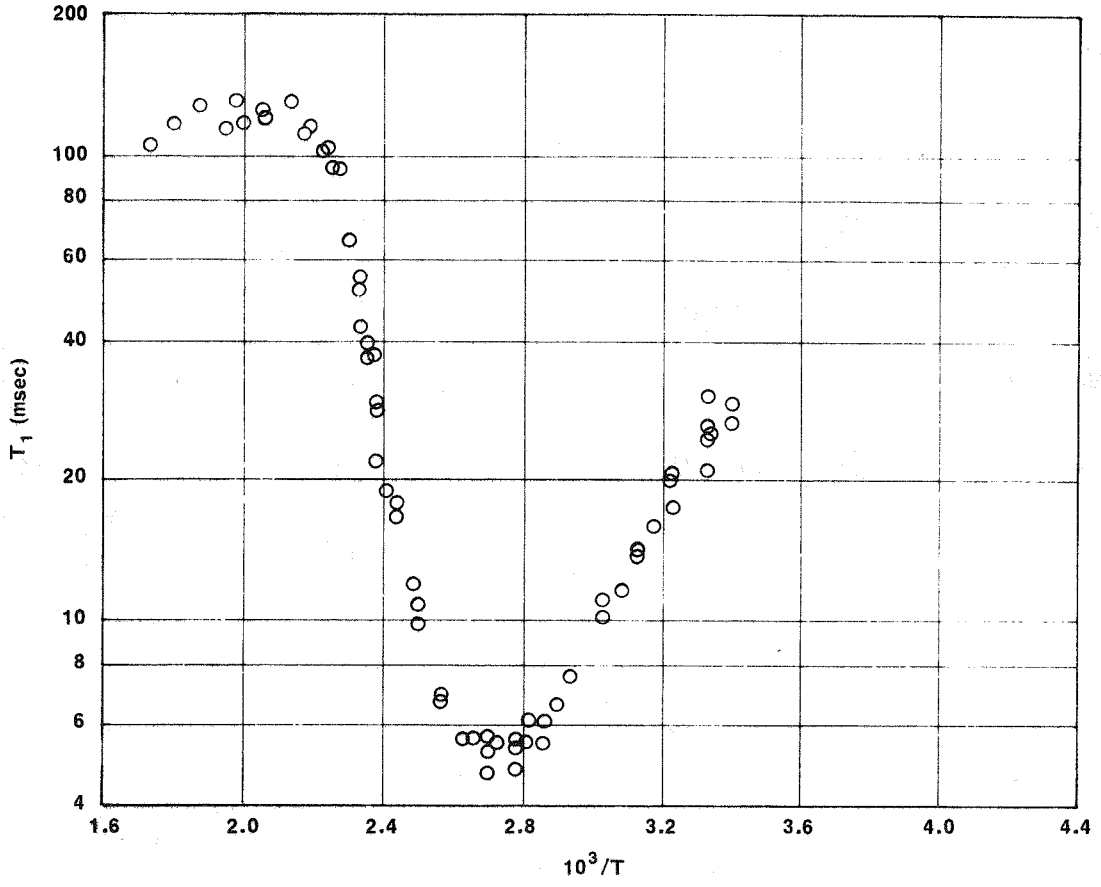

FIGURE 9 - Temperature dependence of the spin-lattice relaxation time T_1 for protons in $VH_{0.53}$ at 23.30 MHz.

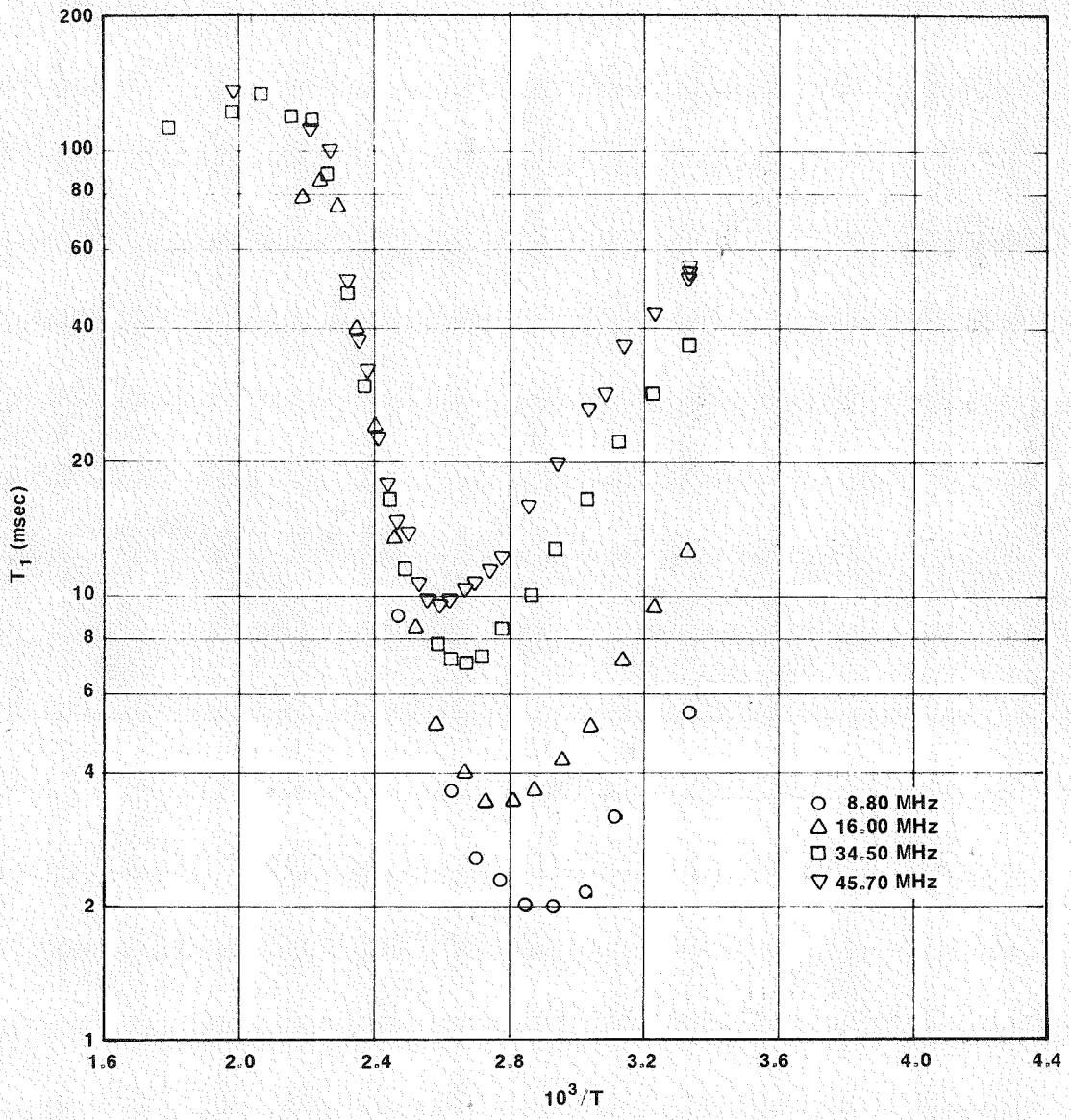

FIGURE 10 - Temperature and resonance frequency dependences of the spin-lattice relaxation time T_1 for protons in $VH_{0.53}$.

$$T_{1d}^{-1} = \left(\frac{2}{5}\right) \frac{C_S}{\omega_I} \frac{110.2}{a_o^6} \left[\frac{\frac{1}{3} y_I}{1 + (y_I - y_S)^2} + \frac{y_I}{1 + y_I^2} + 1 + \frac{2_I}{(y_I + y_S)^2} \right], \quad (3)$$

where $y_I = 1/\omega_I \tau_c$ and $y_S = 1/W_S \tau_c$. The minimum value of T_{1d} can be obtained by setting the derivative of Eq. (3) to zero and solving for y_I. This calculation has been performed, and the minimum occurs when $\omega_1 \tau_c = 0.922$. After some algebra, the expression for (T_{1d}) min for $VH_{0.53}$ is:

$$\left(\frac{1}{T_{1d}}\right)_{min} = \frac{15.18\ C_I}{\nu_o a_o^6} , \quad (4)$$

where ν_o is the proton resonance frequency in units of Hz.

The experimentally determined minimum T_1 values are given as a function of ν_o in Figure 11 along with the minimum T_{1d} values calculated using Eq. (4). The experimental values are approximately twice as large as the theoretical values. Similar discrepancies between experimental values and BPP model values have been observed in previous studies of TaH_x,[7] VCr_yH_x,[8] and ScH_x.[9] Three possible contributions could be responsible. First, the neglect of the metal nuclei quadrupole moment tends to give an overestimation of the metal-hydrogen dipolar interaction. Secondly, the proton jumps to adjacent interstitial sites may be too short for full modulation of the dipolar interactions and the calculated relaxation rates will be overestimated. Finally, the assumptions of the BPP model may be too restrictive to accurately represent the proton diffusion contribution to dipolar relaxation. Unfortunately, a more complete model for metal-hydrogen systems with two different spins has not yet been developed. Nevertheless, Eq. (3) should be adequate to determine τ_c if the data is normalized by using the ratio of T_1 to $T_{1\,min}$ since this general procedure has been satisfactorily applied to several metal hydrides.[7,9-11] Since the experimental $T_{1min} \to 0$ as ν_o decreases, the conduction electron contribution must be small and $T_{1d} \approx T_1$ near $T_{1\,min}$.

The activation energy E_a for proton self-diffusion can be estimated[3,8,12] from a plot of ln T_1 versus $1/T$ for temperatures below the $T_{1\,min}$. This simple procedure does not require the numerical evaluation of Eq. (3). Using the data from Figures 9 and 10, E_a for the $VH_{0.53}$ sample is 0.21 ±0.01 eV. This result is in good agreement

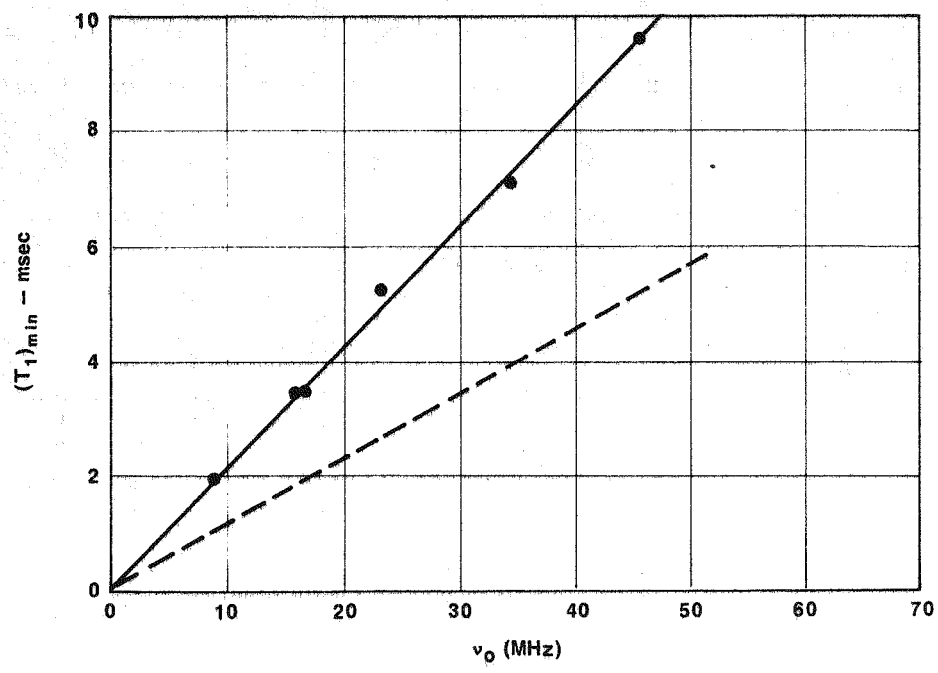

FIGURE 11 - Frequency dependence of the T_1 minimum values for protons in $VH_{0.53}$. The dashed line represents the minimum T_{1d} calculated from Eq. (4).

with previous values for VCr_yH_x[8] and β-phase NbH_x,[12] which have very similar crystal structures, and the hydrogen diffusion characteristics are expected to be similar. However, a more complete analysis of the $VH_{0.53}$ data based upon Eq. (3) is being conducted to determine the τ_c values.

The T_1 studies of proton diffusion in VH_x will be performed on several compositions to determine the effects of phase changes and stoichiometries. The temperature range of these studies will be increased to include lower temperatures and possibly determine any conduction electron contributions to T_1. Proton diffusion in α-phase VH_x will be investigated by spin echo and pulse gradient techniques. Finally, the low-temperature ordering of protons in β-phase VH_x will be investigated.

Studies of $FeTiH_x$ The intermetallic compound FeTi reacts directly with hydrogen to form, in succession, hydrides of approximate compositions FeTiH and $FeTiH_2$. Reilly and Wiswall[13] have determined the disassociation pressures as well as other properties of these hydrides and concluded they would be useful as a hydrogen storage medium. Unfortunately, many other important properties of these hydrides such as crystal structures and hydrogen diffusion parameters have not been determined. Since information on both proton locations and diffusion can be obtained, pulse NMR studies would be very valuable. Consequently, a comprehensive investigation of $FeTiH_x$ by NMR techniques has been undertaken.

Samples of $FeTiH_{1.1}$ and $FeTiH_{1.7}$ were prepared at Mound Laboratory by W. E. Tadlock. The FeTi alloy was prepared by arc-melting under argon. The FeTi button was crushed to -100 mesh powder and exposed several times to hydrogen at 1000 psi overpressure following the general procedures of Reilly and Wiswall.[13] Subsequent x-ray analyses indicated that $FeTiH_{1.1}$ was tetragonal with $a_o = 3.17 \pm 0.02$ Å, and $c_o = 8.78 \pm 0.04$ Å; and $FeTiH_{1.7}$ was cubic with $a_o = 6.60 \pm 0.02$ Å. These results agreed with the data of Reilly and Wiswall for β-phase and γ-phase $FiTiH_x$, respectively.

During the initial NMR studies on the two $FeTiH_x$ samples, no signals were detected when a single π/2-pulse was applied. However, an extremely sharp (that is, $T_2^* = 2$-4 μsec) proton echo was observed when a $\pi/2 - t' - \pi/2$ pulse sequence (with $t' \leq 50$ μsec) was used. Because the electronic recovery time of the spectrometer is ~8-10 μsec, the proton line width relaxation time (T_2^*) is too short for detection after a single pulse. The results of the preliminary measurements for these $FeTiH_x$ samples at room temperature are given in Table 4. Here, T_2^* is the line width decay time; T_2' is the spin-spin relaxation time from the decay of the echo maximum with t'; and T_1 is the spin-lattice relaxation time. Since T_2^* increases with resonance frequency, $T_2^* \ll T_2'$, and T_2' is approximately independent of resonance frequency, the proton echoes are probably inhomogeneously broadened (that is, T_2^* is not only caused by dipolar interactions and lifetime effects, but it also has inhomogeneous field contributions). There are two possible sources of these inhomogeneous fields: intrinsic paramagnetism from the $FeTiH_x$ electronic structure or the presence of impurities such as free iron or iron oxide. However, x-ray diffraction showed no evidence of any other iron compound; but its sensitivity is not very good. Preparation of the hydrides from other batches of the FeTi alloy are planned to determine if impurities are responsible for the inhomogeneous NMR line shapes. The nuclear relaxation times are distinctly different for the two $FeTiH_x$ phases, but it is not yet possible to completely relate the data in Table 4 to the microscopic properties. Since the T_1 values are independent of ν, the main relaxation mechanism must be due to to conduction electrons and not proton diffusion. Furthermore, the short T_2' values indicate that proton self-diffusion in both phases is not rapid enough to significantly reduce the proton dipolar interactions. However, additional measurements to evaluate both proton structure and and diffusion are in progress. In addition, x-ray diffraction studies to determine the crystal structures of both $FeTiH_x$ phases are being conducted.

(R. C. Bowman, Jr.)

Table 4

NMR PARAMETERS FOR $FeTiH_x$ AT ROOM TEMPERATURES

	$FeTiH_{1.1}$ (β-phase)			$FeTiH_{1.7}$ (γ-phase)		
ν (MHz)	T_2^* (μsec)	T_2' (μsec)	T_1 (msec)	T_2^* (μsec)	T_2' (μsec)	T_1 (msec)
45.70	-	32	-	2.4	20	23
34.50	3.3	31	6.5	2.6	20	23
23.30	-	-	-	3.0	20	25
16.00	4.8	26	6.6	3.8	22	24

Separation Chemistry

DISSOLUTION AND RECOVERY OF MASSIVE IRIDIUM IN A NITRATE SYSTEM

Iridium is such an expensive metal that economic considerations often do not allow it to be discarded after use. Because iridium is such a noble and unreactive metal, the recovery of iridium can be a lengthy and laborious process.[14] Moreover, much iridium chemistry is intimately connected with halogens so that established processes for dissolving and recovering massive iridium usually involve halogen. These circumstances are unfortunate when the iridium must be recovered from radioactive debris such as plutonium dioxide since facilities for handling large amounts of radioactivity are often made of stainless steel and hence cannot suffer exposure to halogen without the risk of pronounced corrosion. Moreover, radioactive facilities are often constructed as simply and sturdily as possible, and intricate, involved recovery processes may adapt poorly to such facilities without costly facility modification. It is therefore the purpose of this section to provide a method of dissolving and recovering massive iridium which: is simple in design and operation, uses only commonly available chemicals, avoids halogens entirely, is sufficiently flexible to allow a choice of alternative paths, and is adaptable to the recovery of iridium from radioactive materials such as plutonium dioxide.

Iridium is a noble and unreactive metal; even aqua regia does not attack massive iridium, and it is necessary to resort to high temperatures, high pressures in sealed tubes, and halogen acids for dissolution of iridium. Curiously, a noble metal such as iridium may not be easily reduced to the metallic state once it has been dissolved. Zinc in hydrochloric acid is satisfactory for this reduction; as is formic acid at pH 5, although this technique does not appear to be suitable for the processing of large quantities of iridium even though it might be adaptable to systems in which halogen is absent.

Metallic iridium is converted to an oxide (believed to be IrO_2) by the action of molten potassium hydroxide (KOH), potassium nitrate (KNO_3) mixtures. This oxide of iridium is soluble in hydrochloric acid; but it is not generally recognized, and does not appear to be anywhere recorded, that it can be rendered soluble in nitric acid. When treated with nitric acid, the oxide from the KOH-KNO_3 fusion will sometimes dissolve completely and sometimes only partially. An important ingredient in the dissolution of iridium in nitric acid is the presence of an excess of nitrite or nitrous acid. Alkali metal nitrates lose oxygen upon ignition as illustrated in Eq. (1)

$$KNO_3 \triangleq KNO_2 + \tfrac{1}{2}O_2 \qquad (1)$$

and, if there were a large excess of nitrate in the fusion mixture, sufficient nitrite may have been generated by thermal decomposition of the alkali nitrate to solubilize the oxide of iridium in nitric acid. Often, however, there will be insufficient nitrite present in the fusion mixture, and the following procedure has been used to render iridium soluble in nitric acid (Nitric acid itself may contain nitrous acid and nitrogen oxides formed by decomposition, and this nitrous acid may aid in the dissolution of the iridium oxide). Place a piece of metallic iridium weighing 0.1-0.3 g in a small magnesia crucible and add equal portions of KOH and KNO_3 weighing 3-5 g each. Place the crucible in a furnace and raise the temperature of the furnace to 900-950°C for about 30 min. Cool the crucible and dissolve the solidified melt in 50-100 ml of hot water. Cool the water containing the oxidized iridium precipitate in an ice bath; and when the solution is cool, add sufficient nitric acid to neutralize the KOH. Keep the solution cold, add 0.5-5 g of sodium nitrite ($NaNO_2$) and stir until dissolved. Then, carefully add sufficient 15M nitric acid to raise the acidity of the solution to 2-7M. An acid concentration less than about 2M is not particularly effective for quickly solubilizing the hydrous iridium oxide, and an acid concentration greater than 7M is not necessary. Stir the solution and heat it to the boiling point. Allow the solution to boil until all of the black, hydrous IrO_2 has dissolved to give a green solution. Ordinarily, this takes 10-30 min (Instead of KOH-KNO_3 fusion mixture, a Na_2O_2 fusion may be used

and the iridium dissolved as described above. Pure KNO_3 may also be used, thus sparing the expense and trouble of the potassium hydroxide and the nitric acid later required to neutralize it.)

Using the above procedure, iridium has been routinely dissolved in nitric acid solution without the use of any other chemicals except an alkali nitrate, nitrite, and hydroxide. Since nitric acid neutralizes the hydroxide and since nitrous acid from the alkali nitrite is removed by boiling, the solution that remains contains only iridium, nitric acid, and an alkali nitrate. If the crucible for the fusion is porous, as magnesia crucibles usually are, a small amount of the iridium will penetrate the crucible walls and represent a loss. All of the remaining iridium will be dissolved and appear in the nitric acid solution, however.

While PuO_2, for example, can be solubilized by fusing it with Na_2O_2, this actinide oxide is not known to be rendered soluble by a fusion with KOH + KNO_3 or pure KNO_3. Since refractory PuO_2 is difficult to dissolve in concentrated HNO_3 and since the above described process uses at most 7M HNO_3, that process should solubilize very little PuO_2 (a common radioactive contaminant for iridium). Hence, a partial separation of the iridium from insoluble PuO_2 could be effected by filtering the green iridium solution.

The iridium may be recovered from the solution in any of several ways. One of those ways is the formic acid method described by DUVAL[15] which yields a precipitate of iridium that can be filtered only with difficulty.

Alternate approaches, however, are available:

1. The iridium solution may be adjusted to 7.2M in nitric acid and the solution passed through an anion exchange resin column. This is a well established technique for retaining plutonium in the resin. The resin will allow 75-95% of the iridium to pass through it, however, thus allowing a partial separation of Pu from Ir. The plutonium on the resin may then be removed from the resin with 0.35M nitric acid, leaving only the iridium on the resin. The resin may then be burned or otherwise treated to recover the remaining iridium which, if contaminated, may be reprocessed by fusion as described above.

2. The iridium solution may be evaporated to dryness on a hot plate, and the residue, containing KNO_3 and an unknown iridium salt, baked at a high temperature. This converts the iridium to black IrO_2 which is insoluble in hot nitric acid. For example, after baking at 500°C for 30 min, only about 1% of the original iridium in a sample could be dissolved (after boiling for about 5 min) in a solution of 25 ml of concentrated HNO_3 (15M) plus 5 ml of H_2O.

   Some typical results of this treatment are summarized in Table 5.

   Since PuO_2 is soluble in boiling HNO_3-HF mixtures, this acid treatment may be used to dissolve the PuO_2 away from the acid-insoluble iridium residue.

3. The fusion technique may be modified so that potassium pyrosulfate may be substituted for the KOH, and then a little more KNO_3 added. For example, a weight ratio of $KNO_3/K_2S_2O_7$ of 3/2 may be used to oxidize the iridium. Then, the iridium solution upon drying and baking will contain sulfate. Since sulfate fusions are used to solubilize materials such as PuO_2, the presence of sulfate in the baked residue may help retain the plutonium in a soluble form. In either case, boiling the baked residue with concentrated nitric acid is a technique for dissolving PuO_2 while allowing the iridium residue from the baking step to remain insoluble. Hence, this step may help to further separate the iridium from the plutonium. Alternatively, a sulfate salt such as potassium sulfate (K_2SO_4) may be added to the nitric acid solution of iridium prior to evaporation and baking.

4. In a dilute acid solution, iridium dissolved as described above may be precipitated. Since it did not give a clear x-ray pattern, the precipitated iridium species could not be identified (It is probably hydrous IrO_2; however, that has not been proved). Several oxidants effect this precipitation of iridium from dilute acid when dissolved in the iridium solution and boiled for a few minutes. Among these oxidants are: $KClO_3$, $KBrO_3$, HIO_3, H_5IO_6, and $K_2S_2O_8$ in the presence of a trace of silver nitrate. Table 6 describes some typical results of the oxidation technique.

Since many elements, including plutonium, are not converted to insoluble forms in dilute nitric acid by boiling with an oxidizing agent, this appears to be a good method for separating most elements from iridium. Plutonium is oxidized to the hexavalent state by boiling with $K_2S_2O_8$ (potassium persulfate), a form of plutonium which is quite soluble in acids.

5. The technique of carrier precipitation could also be used to separate soluble plutonium from iridium solutions. For example, thorium could be dissolved in the iridium solutions as thorium nitrate. Then, since both thorium and plutonium form insoluble iodates, precipitation of the thorium as thorium iodate might be effective in carrying most of the plutonium with the thorium iodate precipitate so that a plutonium, iridium separation could be effected in this manner. Other precipitants might be more effective than iodate.

Table 5

RECOVERY OF IRIDIUM FROM NITRIC ACID BY BAKING

Sample No.	Baking Temperature (°C)	Acid Mixture (HNO_3)	Iridium Dissolved (%)
1	500	25 ml conc. +5 ml water	1.0
2	600	25 ml conc. 5 ml water	2.0
3	600	conc. (25 ml)	0
4	600	conc. (25 ml)	0
5	600-650	25 ml +4 drops HF	0.5
6	600-650	25 ml +4 drops HF	1.4
7	600-650	25 ml +4 drops HF	1.0

Table 6

SEPARATION OF IRIDIUM FROM NITRIC ACID BY OXIDATION WITH $K_2S_2O_8$ CATALYZED BY $AgNO_3$ IN 20 ML OF IRIDIUM SOLUTION

Sample No.	HNO_3 Molarity (M)	Weight $K_2S_2O_8$ Added (mg)	Iridium Not Precipitated (%)
1	0.15	1000	0
2	0.26	1000	0
3	0.41	1000	7.1
4	0.51	1000	24.3
5	0.07	200	0
6	0.06	200	0
7	0.10	200	0.14
8	0.15	200	0.10
9	0.20	200	0.36
10	0.26	200	0.96

Four of the techniques for recovering iridium listed above ultimately leave a black residue of iridium which appears to be hydrous IrO_2. This material, whatever its nature, is not appreciably soluble in HNO_3; so that boiling this material with HNO_3 should separate it from most radioactive substances, since the latter are almost always soluble to some extent in boiling HNO_3. To recover metallic iridium from the hydrous IrO_2, it is necessary to reduce the iridium oxide, as, for example, in a hydrogen reduction furnace. But the result of reducing IrO_2 by hydrogen is metallic iridium, a material which is also insoluble in nitric acid. Changing the chemical form and crystal structure of the solid iridium residue by hydrogen reduction may allow entrapped particles of radioactive debris to become exposed. Hence, boiling the metallic iridium from the reduction process with nitric acid may also allow a further separation of the iridium and radioactive substances. *(G. L. Silver)*

PROTACTINIUM-231 AND THORIUM-230

Mound Laboratory is recovering thorium-230 and protactinium-231 from a uranium mill by-product known as Cotter Concentrate and shipping the products to the Heavy Elements Isotope Pool at Holifield National Laboratory (HNL). Previous reports[16,17] have described in detail the origin and character of the Cotter Concentrate, the facilities, and the recovery and purification process. Briefly, the process consists of leaching about 15 liters of solids in hot nitric acid and filtering off the insoluble residue. Uranium is extracted from 90-liter batches of filtrate by multiple contacts with 8-liter portions of 10% DSBPP/CCl_4 (di-sec-butyl phenyl phosphonate in carbon tetrachloride) and stripped from the organic with 0.005M HNO_3. Thorium is preferentially extracted by multiple contacts with 0.1M TOPO/CCl_4 (trioctyl phosphine oxide in carbon tetrachloride) and stripped with 0.3M H_2SO_4. Protactinium is subsequently extracted with TOPO/CCl_4 and stripped out with 0.5M oxalic acid. Uranium strip solutions are precipitated with ammonia, and the precipitate collected for eventual return to a uranium processor. The thorium strip solutions are precipitated, and the thorium is purified by an oxalate precipitation method. Protactinium is recovered from the protactinium strip solutions by precipitation on a manganese dioxide carrier, then purified by standard techniques. The process is summarized by a process flow diagram in Figure 12.

Since November 1974 when the process development work was essentially completed, 30 batches of Cotter Concentrate have been processed. Total volume was 137 gal (519 liters) from four drums but was approximately equal to the contents of three drums (No. 174, 175, and 178). Analyses generated during the processing are compiled and summarized in Table 7.

Table 7

SUMMARY OF PROTACTINIUM AND THORIUM-230 RECOVERY OPERATIONS

	^{231}Pa (g)	%	^{230}Th (g)	%
Total Feed Solutions (from 30 batches)	0.20	41	60	97
Total Strip Solutions	0.25	51	53	85
Estimated Extraction Losses	0.002 per batch 0.06	 12	0.15 per batch 4.5	 7
Estimated Losses In Solids	0.006 per batch 0.18	 37	0.07 per batch 2.1	 3
Total	0.49	100	62	100
Sum of Three Drums (No. 174, 175, 178)	0.58	118	91	146

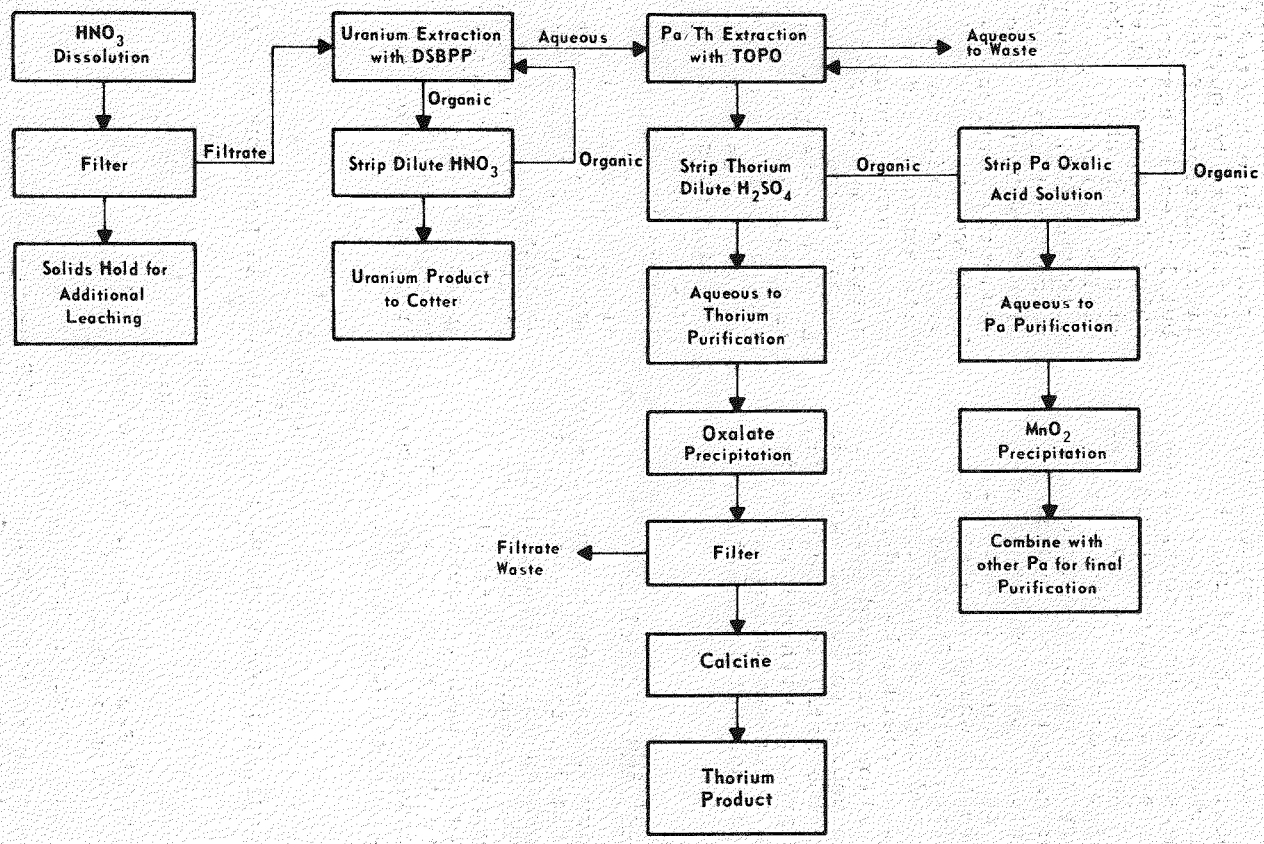

FIGURE 12 - Pa/Th recovery and purification from Cotter Concentrate.

The data on thorium-230, based on the integration of the 68 keV gamma peak, show good consistency. This peak was obtained from 20 ml liquid samples with a low energy photon spectrometer. Some loss of thorium occurs during the uranium extraction, and part of the thorium "tails out" into the protactinium strip solutions and is not included in the summation (and often is not recovered during the processing of the strip solutions). An additional "loss" of thorium to the insoluble residue (filter-aid) occurs, probably due to incomplete washing of the residue, and has been estimated at 3% based on the analysis of the residues from 12 batches. However, these residues are being retained for future processing. Because the final thorium products are always somewhat larger than expected from LEPS counting, the thorium analyses seem to contain a negative bias. From thorium products already analyzed and estimates of material "in process," it is expected that the 30 batches will produce about 70 g of thorium-230. The thorium-230 content of three drums of Cotter Concentrate, approximating the feed material for the 30 batches, showed about 91 g. The difference is due to analytical errors, sampling errors, and approximations. From these data it was concluded that overall thorium recoveries of 90% were being achieved, and the major loss mechanisms have been identified.

The data on protactinium in Table 7 differ from that on thorium in the following respect: The values were obtained by integration of the 27 keV gamma peak from 20 ml liquid samples, assuming a liquid density of one. Since feed solution densities are much higher, and vary from batch to batch, and the self-absorption within the sample of the 27 keV gamma is affected much more by variations in liquid density than the 68 keV gamma of Th-230, the feed solution analytical results average 25% lower than those for the strip solutions, which are better estimates of the true values. Two areas of protactinium loss in the extraction process were recognized and estimated - loss of small amounts of protactinium to the thorium strip solutions, which were not recovered, and the protactinium left in the raffinate solution when the protactinium extraction was stopped. As expected from development work, the fraction of protactinium left on the residues (filter-aid) was quite a bit higher than for thorium. Processing of the protactinium has not proceeded beyond the concentration with manganese dioxide; and a good figure for the total protactinium is not available, but it appears that only half of the potential protactinium is being recovered with nearly 40% loss to the insoluble residues (which are being retained for additional processing). The protactinium content of the three drums, which approximate the material processed, shows about 0.58 g or 20% more than the protactinium found during the processing.

A shipment of 10.11 g of thorium-230 was made to the Heavy Element Pool at HNL in December 1974, and a 40-50 g shipment is being prepared. Final analyses on the second shipment are not yet available. The major impurity found in the thorium-230 product was Sc at 1 to 2% with lesser (0.1% or less) amounts of Zr, Si, P, Na, B, Y, Ca, Mo, Fe, Al, and Cu. The isotopic ratio (thorium-230/total thorium) of the first shipment was found to be 0.03, and the second shipment appears to be the same.

Two Karr three-inch diameter reciprocating plate liquid-liquid extraction columns were received in April 1975 and have been set in place in the SW-140 hot cell. Installation of piping, electrical, and air control connections is underway. Initial operation will be achieved in the first half of FY-1976.

The current processing method for Cotter Concentrate feed solutions entails five liquid-liquid contacts: (1) extraction of uranium, (2) stripping of uranium, (3) extraction of thorium and protactinium, (4) stripping of thorium, and (5) stripping of protactinium. Initial column operation will be for development of operating procedures and determination of parameters for each of the five liquid-liquid contacts. The columns will then be put into operation for those steps which will result in maximum rate of output of thorium and protactinium in the overall operation. Column operation is expected to be at a throughput rate five to ten times that now achieved for the same steps in the small hand-operated batch mixer-settlers now in use. *(P. E. Figgins, M. R. Hertz, W. S. Stringham, and R. M. Watrous)*

STUDY OF THE REACTION OF PLUTONIUM WITH BONE CHAR

One of the principal problems associated with the commercial generation of electric power by nuclear means is the problem of radioactive waste disposal. A study of the reaction of plutonium with bone char, a material commercially prepared from animal bones, has been undertaken to gain some insight into the mechanism by which this material removes plutonium from waste streams. It may be recalled that the extent, rate and mechanism of the solubility of hydroxylapatite (HAP), the principal phosphate of calcium in bone char, and the primary constituent of interest in bone char, is poorly understood.[18] Typical of the papers describing one or more of the theories of hydroxylapatite solubility are those of Zimmerman,[19] and Best and Hearon.[20] But studies of HAP are not limited to studies of the poorly understood water solubility of this material. Other studies of this substance have considered ion exchange reactions of HAP with calcium,[21,22] phosphorus,[23] strontium,[24] and sodium.[25] Additionally, adsorption characteristics of bone char have been examined.[26,27]

Experimental work on the adsorption of plutonium from alkaline aqueous solutions has continued. Early experiments consisted of equilibrating samples of plutonium in an alkaline solution (pH approximately 10) with weighed samples of bone char for a few days, filtering the liquid in contact with the bone char, and counting this liquid after filtration. The purpose of the filtration step was to separate small suspended particles of bone char from the liquid prior to scintillation counting. It was soon observed that with those solutions which had been pretreated with divalent silver oxide (to oxidize the plutonium to the hexavalent state), the mere act of repeated filtering was sufficient to decrease the count rate of the solution. That is, an unfiltered solution had a higher count rate than a once filtered solution, which had a higher count rate than a twice filtered solution, which had a higher count rate than a thrice filtered solution, and so on. Without further investigation, this was attributed to such causes as: a) adsorption of plutonium ions, such as Pu(VI), by the filter paper; b) incomplete filtration of particles of bone char containing adsorbed plutonium; c) incomplete filtration of particles of hydrous Pu(IV) oxide; d) reduction by the organic filter paper of hexavalent or pentavalent plutonium to give adsorbed tetravalent plutonium on the filter paper. Whatever the reason for the decreased count with increased filtration, the phenomenon was sufficient to suggest the desirability of another method of separating soluble plutonium ions form plutonium in the form of particles. Therefore, centrifugation was considered a means of separation.

One milliliter samples of a stock plutonium solution were evaporated to about 1 ml with 10-15 ml of concentrated nitric acid to decompose any polymer which might have been present. A few drops of a nitric acid solution, in which a small amount of AgO had been dissolved, were then added to the samples. This nitric acid solution was added to oxidize the plutonium to the hexavalent state. The solutions were treated with ammonia to raise the pH to about 10. Small portions of the solutions were then counted. Portions of the solutions were then centrifuged at various speeds for 10 min periods. It was found that if a sample was centrifuged @ 5000 rpm for 10 min, the count rate decreased considerably from the count rate of the original solution. At a speed of 10,000 rpm, the count rate decreased further. However @ 15,000 rpm, the count rate decreased only slightly more. Since the plastic centrifuge tubes crack (and thereby release radioactive solution) at speeds much in excess of 10,000 rpm, this speed was selected as the speed suitable for preliminary studies of the reaction of plutonium with bone char.

One of the important parameters determining the behavior of plutonium with bone char is the effect which the bone char exerts upon its environment. In the case of the reaction of plutonium with the commercial bone char studied here, the manner in which the bone char affects the trace of aqueous plutonium is of primary importance. Since alkaline solutions are of interest, several solutions with pH values from about 9 to 11 (with ammonia buffer) were prepared. Each 100 ml buffer also contained a weighed 1 g sample of commercial bone char. After a five-day equilibrium period, during which the samples (in 100 ml volumetric flasks) were shaken repeatedly, the pH and electromotive force values of the solutions were measured (EMF values were taken using a ferricyanide/ferrocyanide buffer assigned a potential value of +0.41 V.)

The above experiments were repeated and repeated once again with a carbonate/bicarbonate pH buffer. Figure 13 shows the results with an ammonia/ammonium nitrate buffer, Figures 14 and 15 with an ammonia/ammonium chloride buffer, and Figures 16 and 17 with a potassium carbonate/bicarbonate buffer. In each

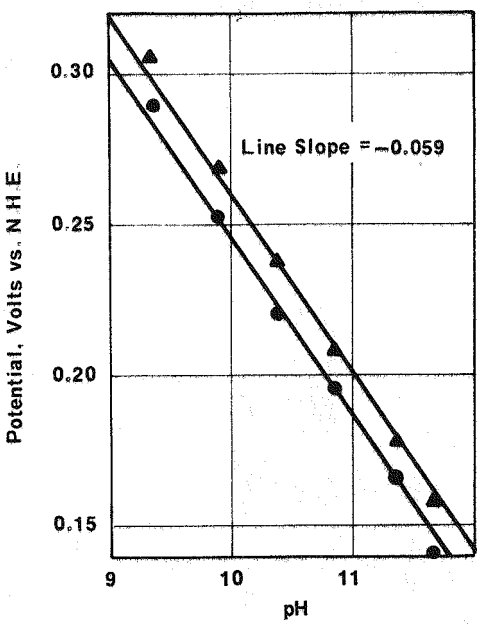

FIGURE 13 - The bone char water system in an NH_3-NH_4NO_3 buffer.

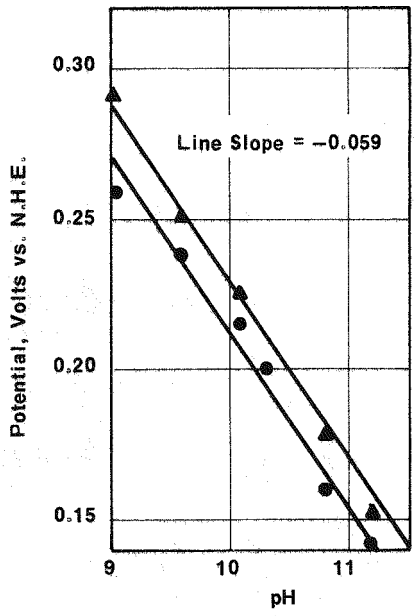

FIGURE 14 - The bone char water system in a moderate amount of NH_3-NH_4Cl buffer.

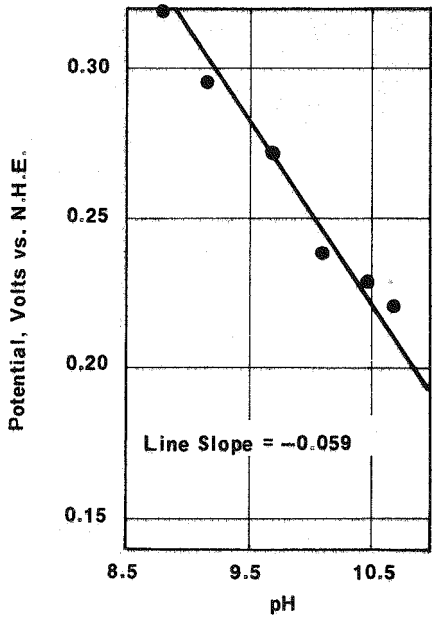

FIGURE 15 - The bone char water system in a small amount of NH_3-NH_4Cl buffer.

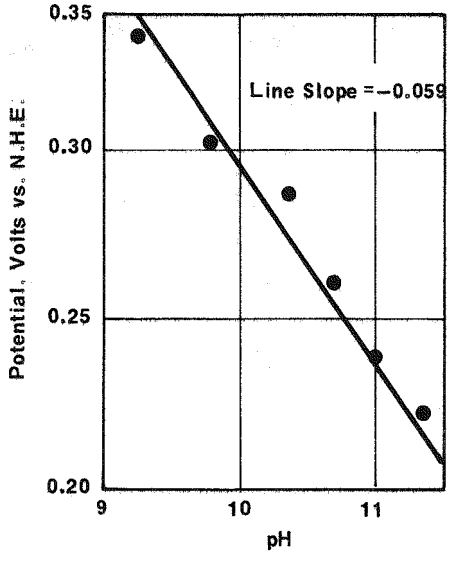

FIGURE 16 - The bone char water system in a $CO_3^{=}$ buffer.

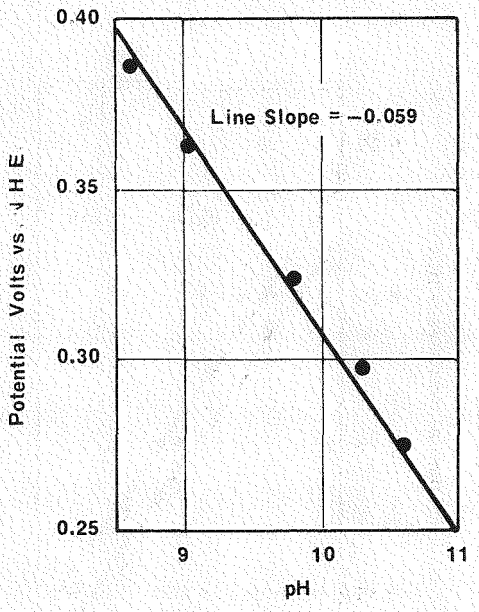

FIGURE 17 - The bone char water system in a HCO_3-buffer.

diagram, the points drawn as circles (lower line) represent the potential pH values of solutions as measured about two minutes after uncapping the samples. Points marked with ▲'s (upper line) were taken after about three minutes of stirring while exposed to atmospheric oxygen (that is, about five minutes after uncapping the sample). In these experiments, it is the potential, not the pH, which changes upon exposure to the atmosphere. In all of the diagrams, lines with a given slope of -0.059 are passed through the points. A line with slope ±0.059 is the theoretical Nernstian value (@ 25°C) for a reversible reaction involving a proton/electron ratio of unity. Other possible, likely values of the absolute value of the slope are the factor ±0.059 times some simple number or fraction such as 1/2, 2, 4/3, 1/3. Since bone char is known to contain organic matter from animal bones, there is no other way of predicting the value of the slope. The points seem to follow the slope -0.059 quite well, however, suggesting that the potential controlling reaction is of the form of Eq. (1):

$$Ox + ne = Red - nH^+, \qquad (1)$$

where "Ox" and "Red" represent the oxidized and reduced forms of the potential controlling reaction, and "e" represents an electron.

The plots in Figures 13-17 suggest certain properties of the bone char/water system. Among these are:

(a) Bone char imposes a low potential upon aqueous systems. At pH 10 this potential for fresh solutions is about +0.25 V, a value characteristic of some organic systems.

(b) The behavior of the potential controlling reaction appears to be poorly reversible and appears to follow the form suggested by Eq. (1).

(c) The fact that the potential drifts slowly upward upon long exposure to atmospheric oxygen implies that the system is oxidized by air, and that the poising capacity of the bone char/water system is very low.

After the potential-pH behavior of the bone char/water system (at pH approximately 10) had been illuminated, the reaction of bone char with the hexavalent oxidation state of plutonium was examined. The hexavalent state of plutonium was selected because: a) It does not polymerize or precipitate, so far as is known, at the concentrations and pH values employed; b) There are standard methods of preparing Pu(VI); c) The general plutonium equilibrium problem predicts that Pu(V), easily prepared from Pu(VI), has a wide "stability" range near the potential-pH region which bone char imposes upon water solutions; d) Pu(III) is likely to be oxidized to insoluble Pu(IV) hydrous oxide at pH 10; and e) Pu(IV) is not appreciably soluble at pH 10, since it quite easily forms a low soluble "polymer" in this low acidity. Of the several methods for preparing Pu(VI) from Pu(IV), treatment with divalent silver oxide was selected.

Samples of silver-oxidized plutonium were allowed to equilibrate with 1 g of bone char in 100 ml of water at selected pH values. Typical results from such experiments are shown in Table 8. Table 8 also gives data on the observed potential values, pH values, and count rate of each solution. Sample No. 6-10 were prepared from the same stock, and to each of these samples was added a few drops of a 0.1M potassium ferricyanide and 0.1M potassium ferrocyanide solution. This was done to effect a potential change at constant acidity. Sample No. 9 and 10 contained most of these complex iron cyanides which produced a yellow precipitate in these samples. For this reason, the data from these samples were questionable.

Table 8

REACTION OF PLUTONIUM WITH BONE CHAR

Solution No.	Count Before Centrifuge[a]	Count After Centrifuge[a]	Net Count Rate After Bone Char[b]	Pu Molarity	Observed Solutions Potential (V)	Solution Acidity (M)
1	13,633	13,487	14.4	15.93E-16	0.250	1.00E-10
2	14,785	14,435	12.2	13.49E-16	0.275	3.09E-10
3	23,149	20,999	32.4	35.83E-16	0.245	5.13E-11
4	23,671	22,766	24.6	22.21E-16	0.262	1.66E-10
5	21,255	10,595	32.2	35.61E-16	0.232	3.00E-11
6	15,064	8,363	75.0	82.95E-16	0.270	1.42E-10
7	[c]	[c]	27.0	29.86E-16	0.252	1.42E-10
8	[c]	[c]	14.6	16.15E-16	0.238	1.42E-10
9	[c]	[c]	10.2	11.28E-16	0.265	1.42E-10
10	[c]	[c]	4.6	5.09-E-16	0.235	1.42E-10

[a] Centrifuged @ 10,000 rpm for 10 min. Count rate = dis/500λ/min.

[b] Disintegrations per minute per milliliter above background.

[c] Solution No. 6-10 prepared from one common stock and contained iron cyanides.

Table 9 shows that bone char is very effective in removing silver-treated plutonium, hereinafter called hexavalent plutonium. The number of counts per minute per ml of a bone char-treated plutonium sample is so low that the standard deviation of the counts is an appreciable fraction of the absolute count rate. Since the entries in col. 4 of Table 8 are net counts per minute per milliliter for a 100 min count (the limit of our instrumentation), the statistics of counting are computed on this basis. Thus the number 14.4 dis/min/ml, which is the first entry in col. 4, represents a gross sample count of 9000 against a background count of 7560. Hence, the 95% confidence level of the first entry in col. 4 is about 14.4 ± 2.6.

One of the interesting aspects of the bone char plutonium reaction is the nature of the equilibrium established between bone char and plutonium in its various forms. One possible equilibrium is that established among the species Pu(VI)-Pu(V)-$Pu(OH)_4$, an equilibrium which was first examined several years ago by Silver.[28,29] To illustrate this equilibrium, consider the approach outlined in ref 28:

$$2PuO_2^+ + 2HOH = PuO_2^{2+} + Pu(OH)_4 \quad K=KP \qquad (2)$$

$$KP = Z/Y^2 = M/Y, \qquad (3)$$

where Z represents PuO_2^{2+} and Y represents PuO_2^+. Then the total soluble (noncentrifugeable) plutonium (T) is closely given by the sum of soluble hexavalent and pentavalent plutonium:

$$T = Y(AY) + Z(AZ) \qquad (4)$$

$$T = (M/KP)(AY) + (AZ)(M^2/KP), \qquad (5)$$

where M is the Z/Y ratio. In other words,

$$\frac{(T)(KP)}{M} = (AY) + (AZ)(M), \qquad (6)$$

and Eq. (6) is amenable to a least squares treatment since T and M can be determined for each solution in Table 8. The value of KP is about 1.89E+04. But examination of Table 9, which gives the values of some parameters in Eq. (6), shows that only for solution No. 6, 7, and 8 are the values of both AY and AZ positive numbers. Their respective values are about 7 and 6E+12, values which at first glance, at least, appear reasonable. Other entries in Table 9 do not seem to fit this model, giving, for example, negative values of AY and AZ. Physically, this is not possible, and suggests that the Pu(VI)-Pu(V)-$Pu(OH)_4$ equilibrium does not represent the equilibrium in the plutonium-bone char system at pH 10. Table 9 suggests another possibility. It is interesting that only those solutions which contained traces of ferricyanide and ferrocyanide gave reasonable values for AY and AZ. This may merely imply that complex cyanides of iron (which are recognized as good complex forming agents) disturb the plutonium-bone char system, so that measurements on systems containing complex cyanides of iron do not accurately represent the equilibrium in the plutonium-bone char system. This problem will be revisited at a later time; for the present, it is sufficient to observe that bone char seems to be very effective in removing hexavalent plutonium from aqueous solutions. Since hexavalent plutonium is one of the four possible oxidation states which can occur in wastewaters, this is a sanguine start. *(G. L. Silver)*

Table 9

METHOD FOR ESTIMATING ALPHA COEFFICIENTS FOR PENTAVALENT (AY) AND HEXAVALENT (AZ) PLUTONIUM

Solution No.	T	M	(T)(KP)/M
1	15.93E-16	5.44E-12	5.53
2	13.49E-16	1.44E-11	1.77
3	35.83E-16	4.48E-12	15.1
4	27.21E-16	8.68E-12	5.93
5	35.61E-16	2.70E-12	24.9
6	82.95E-16	1.18E-11	13.3
7	29.86E-16	5.88E-12	9.60
8	16.15E-16	3.41E-12	8.95

STUDY OF THE REACTION OF URANIUM WITH BONE CHAR

Introduction The objective of this program is to study the mechanism of the reduction of uranium in waste streams to ultra low levels. Emphasis is placed on a process being developed at Mound Laboratory which involves the removal of the uranium from solution by contact with a bed of calcium phosphate. Because of the practical difficulty of filtering pure precipitated $Ca_3(PO_4)_2$, the phosphate used in the process is actually bone char (a natural calcium hydroxyapatite). The process appears to be based on the principle of residue adsorption. According to this principle, trace quantities of inorganic compounds that would precipitate if they were present at the macroscopic level will adsorb quantitatively on nonreactive surfaces if the microcrystals are brought into close enough contact with those nonreactive surfaces. As a corollary to this principle, if the inorganic compound is not insoluble but is brought into intimate contact with a reactive surface, which converts it to an insoluble compound, the inorganic cation will remain attached to that surface. During FY-1975, a study of the reaction between uranium and bone char was initiated. A literature search was conducted to find all information relative to the bone char. Typically, bone char has been used in decolorizing crude sugar syrups and in removing salts from process streams. It has also seen considerable use in removing fluorides from drinking water. Some of its properties include:

1) Internal porosity = 50-55%

2) External void fraction = 18

3) Bulk dry density = 40 lb/ft^3

4) Surface area = 100-115 m^2/g

Adsorption Isotherms The adsorption isotherm is the relationship, at a given temperature and other conditions, between the amount of a substance adsorbed and its concentration in the surrounding solution. If a radioactive isotope (^{234}U) adsorption isotherm is taken, the adsorption isotherm would consist of a curve plotted with residual activity in the water as the abscissa and the activity adsorbed per gram of bone char as the ordinate. A reading taken at any point on the isotherm gives the amount of activity adsorbed per unit weight of bone char, which is the bone char adsorptive capacity at a particular activity concentration and water temperature. In very dilute solutions, such as wastewater, a logarithmic isotherm plotting usually yields a straight line. In this connection, a useful formula is the Freundlich equation which relates the amount of impurity in the solution to that adsorbed as follows:

$$x/m = kC^{1/n},$$

where:

x = amount of activity adsorbed

m = weight of bone char

k and n are constants

C = unadsorbed concentration of activity left in solution,

in logarithmic form:

$$\log x/m = \log k + 1/n \log C,$$

in which 1/n represents the slope of the straight line isotherm.

From an isotherm test, it can be determined whether or not a particular degree of radioactive removal can be effected by adsorption alone. An isotherm test will also show the approximate adsorptive capacity of the bone char for the application and afford a convenient means of studying the effects of pH and temperature on adsorption.

The isotherm plot should be linear but frequently deviates from this ideal. Straight lines may be drawn through many data sets without trouble, and individual deviant points may be discarded as a matter of judgment. Nonlinear or completely scattered sets may require a least-squares fitted line; however, it could be argued that any data set that truly requires a least-squares line is probably worth redoing. Consequently, the success of isotherm testing rests with strict attention to procedural detail.

Once a straight line of fair precision has been drawn, it is extrapolated towards the right to the Co intercept; and the resulting ordinate is a measure of adsorptive capacity.

Experimental Results In order to measure the adsorptive capacity of uranium on bone char, a series of experiments were conducted. Equilibrium tests were run using varying concentrations of bone char along with a constant concentration ^{234}U isotope. The solutions were buffered at pH 10 (NH_3 buffer) to compensate for the buffering capacity of the bone char. The uranium in solution has many possible forms including:

1) UO_2^{+2}

2) Complex with PO_4^{-3}

3) Complex with NH_4OH to form $(NH_4)_2 U_2O_7$

4) Dimer $(UO_2)_2(OH)_2^{+2}$

5) Trimer $(UO_2)_3(OH)_5^{+}$

Presently, it is impossible to conclude which form is the dominant one. The results were plotted (see Figure 18), and a straight line isotherm was obtained via a least-squares treatment of the data. Interpretation of the isotherm gave the following results:

slope = 1.214

intercept = 20.375

capacity of bone char = 67,503 dis/min/mg

Performing a simple linear correlation gave a correlation coefficient of r = 0.99986 for the data.

The adsorption capacity that bone char exhibited for uranium is quite high. The high slope of the isotherm indicates that good adsorption of uranium is obtained at high concentrations but not at low concentrations. Furthermore, this high slope indicates that greater adsorption efficiency in column operation can be expected. *(J. Koenst)*

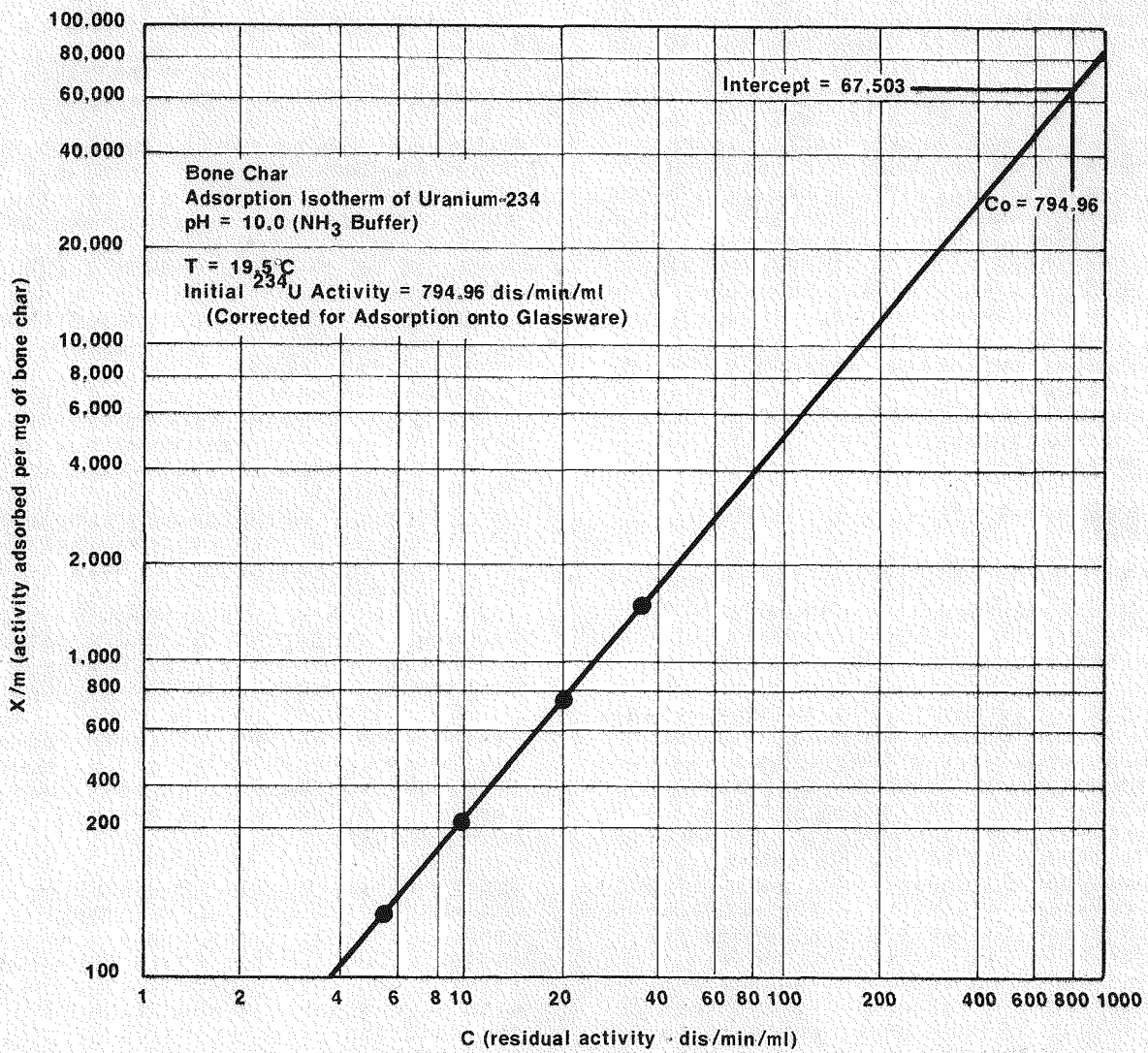

FIGURE 18 - Bone char adsorption isotherm of uranium-234.

THORIUM-229

During this report period, the flow rates and extraction conditions for large quantities (100 g) of ^{233}U established during CY-1974 were successfully applied for the separation of 22.36 mg ^{229}Th from aged ^{233}U. A portion of this amount (1.63 mg) was ^{229}Th separated from previously processed ^{233}U. This will result in a product low in ^{232}Th which should have been removed during the first extraction.

The yield of ^{229}Th on the reextraction was considerably lower than the yield obtained from processing aged ^{233}U containing ^{232}Th. The theoretical amount of ^{229}Th in this reprocessed ^{233}U was 4.95 mg. The ^{232}Th may act as a carrier for the ^{229}Th, increasing the yield. Work to obtain pure ^{229}Th will continue since this product is in great demand by users.

Tests are underway to increase the purity of ^{229}Th product by absorption of the ^{229}Th from the aqueous solution after the ^{233}U has been removed on anion exchange resins in 8M HNO_3 feed. Experiments using 5 mg quantities of ^{230}Th as a stand-in have been run to determine the conditions necessary to absorb and strip thorium ions from the anion exchange column. Contamination of the resin by DSBPP (di-sec-butyl pehnyl phosphonate) and extended stripping time for thorium will be investigated. As expected, ^{230}Th was recovered quantitatively (90% was collected in the first 25 ml of eluant). *(W. S. Stringham and R. M. Watrous)*

URANIUM-234

Mound Laboratory has been separating and recovering high isotopic purity ^{234}U from aged ^{238}Pu materials for several years. Part of the ^{234}U comes from ^{238}Pu "cows" which are held exclusively for the production of ^{234}U. Sometimes the ^{238}Pu recovery operations have processed aged ^{238}Pu heat sources, and by special techniques have produced a relatively concentrated uranium fraction which then becomes the feed material for ^{234}U recovery.

The chemical procedures for separating and purifying the ^{234}U have been described previously;[30] but briefly the process consists of three separation stages, each conducted in a separate hoodline with successively lower levels of plutonium. In the initial separation stage, the bulk of the plutonium is removed by homogeneous oxalate precipitation, leaving the uranium in solution. In the intermediate separation stage, both uranium and plutonium are loaded onto an anion exchange resin from a nitrate medium; and the uranium is selectively washed off the resin. In the final purification step, both uranium and plutonium are loaded onto an anion exchange resin from a hydrochloric acid medium; and the last traces of plutonium are washed off with the aid of a reducing agent.

The first precipitation of plutonium as the oxalate from solution A13-B was described in the last report.[31] This solution was estimated to contain 22 g uranium with 5 g plutonium. This precipitate was combined with the oxalate precipitate from an earlier processing of A13 material. These combined precipitates were dissolved in 2M HNO_3, and the plutonium was reprecipitated to separate any remaining trace of uranium. Precipitation was made with dimethyl oxalate in the presence of H_2O_2 to keep the plutonium reduced. After filtering onto a coarse glass-fritted filter and drying, the plutonium oxalate was set aside for eventual calcination to the oxide and storage as a "cow" designated A13-0.

The uranium-rich filtrates from the first oxalate precipitation (solution A13-B) and the final precipitation described above were evaporated to a convenient volume with an acid concentration of 5.5M. Analysis of the filtrate for plutonium indicated 244 mg ^{238}Pu. Since an acid concentration of 0.3M HNO_3 is desired for the intermediate separation by anion exchange, the filtrate was denitrated with formic acid to a 4.6M acid concentration. A greater reduction in nitrate could not be achieved with this denitration procedure. Final adjustment to 0.3M HNO_3 was accomplished with the addition of concentrated NH_4OH. This solution was also salted to 1.6M $Al(NO_3)_3$ in preparation for the intermediate separation step. Another solution (A13-B2) from which the plutonium was previously precipitated contained an estimated 11 g uranium with 29 mg plutonium. This solution was also adjusted to 1.6M $Al(NO_3)_3$/0.3M HNO_3 in preparation for the intermediate separation step.

The salted solutions were loaded onto the Dowex 1X4 anion exchange resin (nitrate form) in five separate runs to avoid exceeding the capacity of the column for uranium. After each loading, the resin was washed with 1.6M $Al(NO_3)_3$/0.3M HNO_3 solution and the uranium eluted with 7M HNO_3. Finally, the plutonium was eluted with 0.35M HNO_3 containing a small quantity of hydroxlamine nitrate to reduce

the plutonium. Alpha pulse height analyses of the uranium fractions indicated a total of approximately 28.5 g ^{234}U with 43 mg ^{238}Pu. Portions of the raffinates and washes from two of the runs were recycled through the resin, but only a few additional milligrams of uranium were separated. The remaining raffinates and washes were not recycled.

In preparation for the final separation step, anion exchange in a chloride medium, the uranium fractions were combined and evaporated to near dryness. The solids were dissolved in 9M HCl, and an attempt was made to denitrate with formic acid. After several days of this denitration operation, the nitrate was still not all decomposed. Finally, the uranium was precipitated with concentrated NH_4OH and dissolved in 9M HCl three successive times to complete the removal of nitrate. Hydrazine dihydrochloride was added to the final uranyl chloride solution as a reductant for the plutonium.

The uranyl chloride solution was loaded onto the Dowex 1X4 anion exchange resin (chloride form) in four separate runs. Before it was loaded onto the resin, about 2.5% HI was added to each feed solution to keep the plutonium reduced and prevent its loading as much as possible. After each loading, any plutonium that remained was eluted with 9M HCl/2.5% HI; and the column was then washed with 9M HCl. The uranium was eluted with 0.1M HCl. An intermediate fraction of neptunium-237 was also eluted ahead of the uranium with 4.5M HCl. Alpha pulse height analyses of the uranium fractions from the four runs indicated approximately 19 g of ^{234}U with 1-2 ppm ^{238}Pu.

The intensive use of HI as a reductant for the plutonium to improve the separation appeared very effective. But after the first run, about 7 g of uranium was distributed through the raffinates, washes, and neptunium fractions. It appeared that an excess of iodine may have reduced the capacity of the resin and prevented complete loading of the uranium. Therefore, the column was loaded with fresh resin; and the raffinates, washes, and neptunium fractions from the last three runs were recycled. Since analysis indicated the uranium content of the neptunium fractions contained only 1-2 ppm ^{238}Pu, these fractions were adjusted to 9M HCl and loaded first. After loading, the resin was washed with 9M HCl, the neptunium eluted with 4.5M HCl, and the uranium eluted with 0.1M HCl. Again, the uranium was distributed through the raffinate, wash, and neptunium fraction; and essentially no uranium was separated. Next, the raffinates and washes from the last three of the original four runs were loaded onto the fresh resin. No additional HI was added to these solutions before loading. After loading, the column was washed with 9M HCl/1.25% HI and with 9M HCl. A neptunium fraction was eluted with 4.5M HCl, and a uranium fraction was eluted with 0.1M HCl. Again, the uranium was distributed through the raffinate, wash, and neptunium fraction with essentially no uranium being separated. There is a possibility that the uranium formed a compound with H_3PO_2, which is sometimes used as a stabilizer in HI. Also, there is a method which reportedly separates plutonium from uranium by a homogeneous precipitation of uranium with H_3PO_2.[32] The solutions from these recycle attempts will be held for later separation, possibly employing the precipitation method reported.

The uranium products from the four initial separations on the final anion exchange column were precipitated with concentrated NH_4OH, filtered, dried, and calcined to U_3O_8. Total oxide weight of this uranium product, designated A13-2, was 22.285 g. Mass analysis indicated 99.08% ^{234}U, 0.08% ^{235}U, 0.06% ^{236}U, and 0.79% ^{238}U with some mass 237 observed. Alpha pulse height analysis, impurity analysis, and calorimetry have not been completed so a calculated weight of ^{234}U is not yet available. Preliminary results of the alpha pulse height analysis indicated a ^{238}Pu content of 28 ppm which was in sharp disagreement with the analyses of the uranium fractions precipitated. At this time, there is no logical explanation for this disagreement. The oxide will be shipped as soon as the analytical work is completed. *(P. L. Keister, P. E. Figgins, and R. M. Watrous).*

Separation Research

CALCIUM ISOTOPE SEPARATION

Chemical Exchange A prototype chemical exchange system using a Karr reciprocating-plate counter current extraction column and reflux equipment was operated at total reflux for the enrichment of the calcium isotopes. The polyether dicyclohexyl 18-crown-6 was used for the calcium isotope exchange reaction. After withdrawal from the column, the organic phase was stripped of calcium and recycled. The emulsion formed during stripping was effectively reduced by controlling the energy input and stripping water to the mixer. The resultant organic recycle stream contained a minimum quantity of calcium chloride; this parasitic calcium flow is acceptable. Also during the total reflux operation, the interface in the top reflux system was stabilized using the capacitance probe and the interface level controller. Two problems occurred which made the total reflux operation unsatisfactory. The calcium chloride holdup varied in the top reflux system. This resulted from poor temperature control and evaporator design. A proportional temperature controller and a new evaporator-condensor were installed to alleviate this situation. The small density difference between the two phases led to flooding at very low throughputs. A bromoform-chloroform mixture is presently being studied to increase the density difference between the two phases. *(B. E. Jepson and R. W. Hurd)*

LIQUID THERMAL DIFFUSION

An experimental liquid thermal diffusion cascade is being used to enrich sulfur-34 to concentrations greater than 90%. Carbon disulfide is used as the working fluid. The natural abundances of the sulfur isotopes and of the major isotopically substituted species of CS_2 are given in Table 10.

At present, the liquid thermal diffusion system comprises 12 columns arranged in a dual cascade (Figure 19). The mixed molecule $C^{32}S^{34}S$, which does not undergo isotopic exchange at column conditions, is enriched in the first cascade of 7 columns from natural abundance (8%) to approximately 60%. The partially enriched material from the first cascade is passed through an exchange reactor to establish isotopic equilibrium among the various species of carbon disulfide. The exchanged carbon disulfide, now containing an increased concentration of the doubly substituted species ($C^{34}S^{34}S$), is fed to an intermediate point in the second (5-column) cascade; and a product stream highly enriched in $C^{34}S^{34}S$ is removed from the bottom of the second cascade.

The dimensions and operating temperatures of the thermal diffusion columns are given in Table 11. Figure 20 is a simplified schematic cross section of a typical column. The hot wall temperature is established by condensing steam at 7 atm, and the cold wall temperature is maintained by a carefully controlled flow of cooling water. Each column is equipped with cooling water flow distributors at the inlet and outlet points. The first three columns of the first cascade, with a spacing of 300 μm between hot and cold walls, are operated at a coolant flow rate well within the turbulent region. The remaining columns of the system are operated at flow rates corresponding to a Reynolds number of 1500 in the laminar flow regime.

Thermal diffusion column theory predicts that the initial transport coefficient (H) is related to the column spacing between hot and cold walls by:

$$H \propto a^3, \qquad (1)$$

where a is the spacing, and the separation factor at total reflux, q, by:

$$\ln q \propto L/a^4, \qquad (2)$$

where L is the length of the column. Estimated values of these coefficients are given in Table 10.

The columns are arranged in the two cascades so that columns having a high value of the initial transport rate and a low value of the separation factor at total reflux, are placed near the feed point. Columns with a high separation factor and low transport rate conversely, are placed toward the product end of the system. According to isotope separation cascade theory, this arrangement improves the

Table 10

NATURAL ABUNDANCES OF SULFUR AND CARBON ISOTOPES
AND OF ISOTOPICALLY SUBSTITUTED CARBON DISULFIDE MOLECULES

Component	Atom Percent	Component	Mole Percent
^{32}S	95.06	$^{12}C^{32}S^{32}S$	89.40
^{33}S	0.74	$^{12}C^{32}S^{33}S$	1.39
^{34}S	4.18	$^{12}C^{32}S^{34}S$	7.86
^{36}S	0.0136	$^{13}C^{32}S^{32}S$	0.994
		$^{13}C^{32}S^{34}S$	0.087
^{12}C	98.9	$^{12}C^{33}S^{34}S$	0.061
^{13}C	1.1	$^{12}C^{34}S^{34}S$	0.173
		$^{13}C^{34}S^{34}S$	0.0019
		$^{12}C^{32}S^{36}S$	0.026
		$^{12}C^{34}S^{36}S$	0.0011

Table 11

PARAMETERS OF LIQUID THERMAL DIFFUSION COLUMNS
IN THE SULFUR ISOTOPE SEPARATION SYSTEM

Cascade	Column	Spacing (μm)	Annular Diameter (mm)	Length (m)	$10^4 H_o$ [a] (g sec^{-1})	LN q [b]
I	1	300	25.4	2.4	1.09	0.75
	2	300	25.4	2.4	1.09	0.75
	3	300	25.4	2.4	1.09	0.75
	4	250	25.4	0.76	0.47	0.53
	5	250	25.4	0.76	0.47	0.53
	6	250	25.4	0.76	0.47	0.53
	7	250	25.4	0.76	0.47	0.53
II	1	250	25.4	0.76	0.47	0.53
	2	250	25.4	0.76	0.47	0.53
	3	250	25.4	0.76	0.47	0.53
	4	250	19.1	0.60	0.35	0.53
	5	180	19.1	0.91	0.12	2.30

Steam temperature: 164°C
Water Temperature: 20°C

[a] Initial transport coefficient based on one unit difference in mass.

[b] q is the separation factor at total reflux for one unit difference in mass.

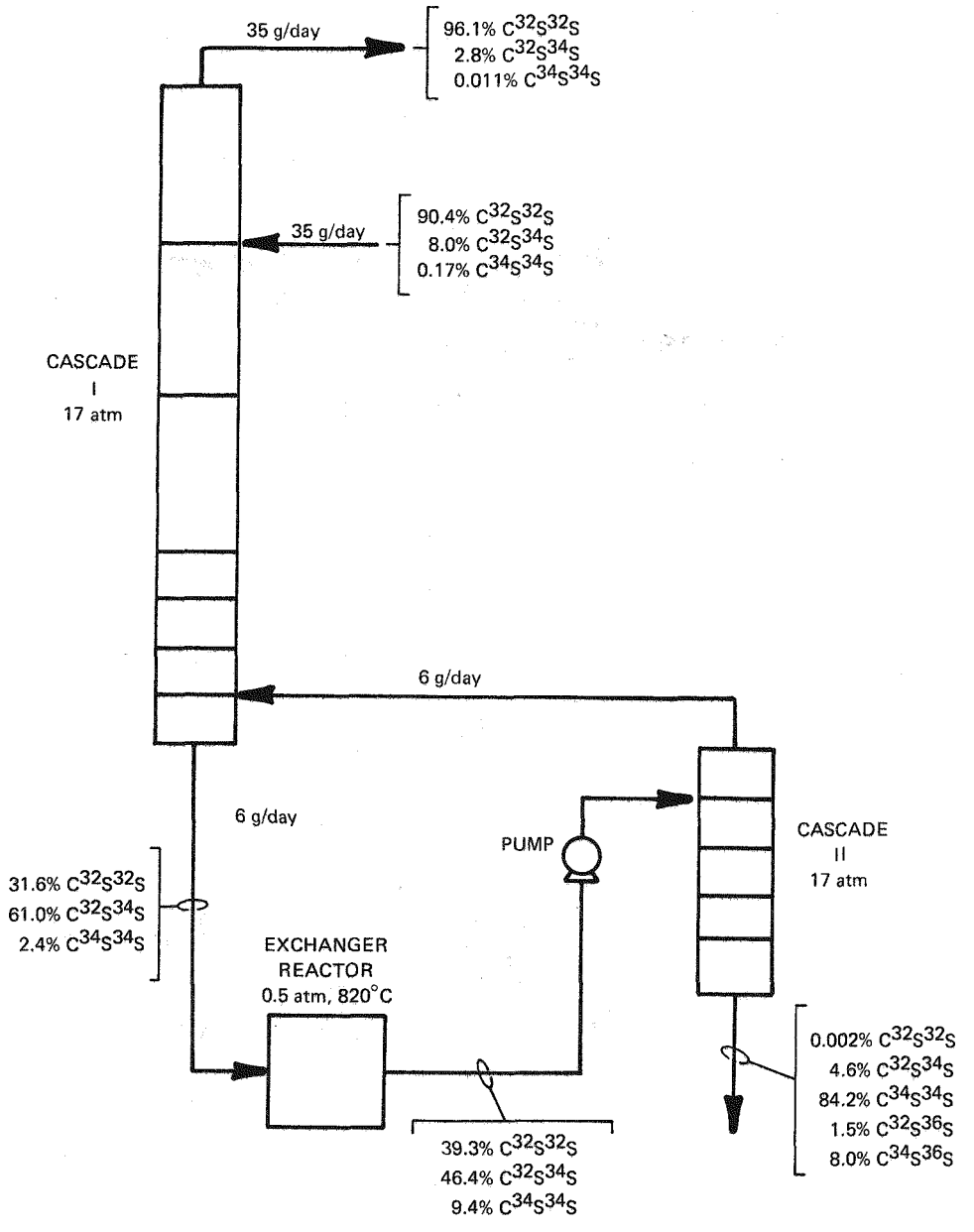

FIGURE 19 - The liquid thermal diffusion system, showing the calculated conditions prevailing at the first time step after 90% ^{34}S is reached (each rectangle represents a column, and the height of each rectangle is proportional to the length of the column).

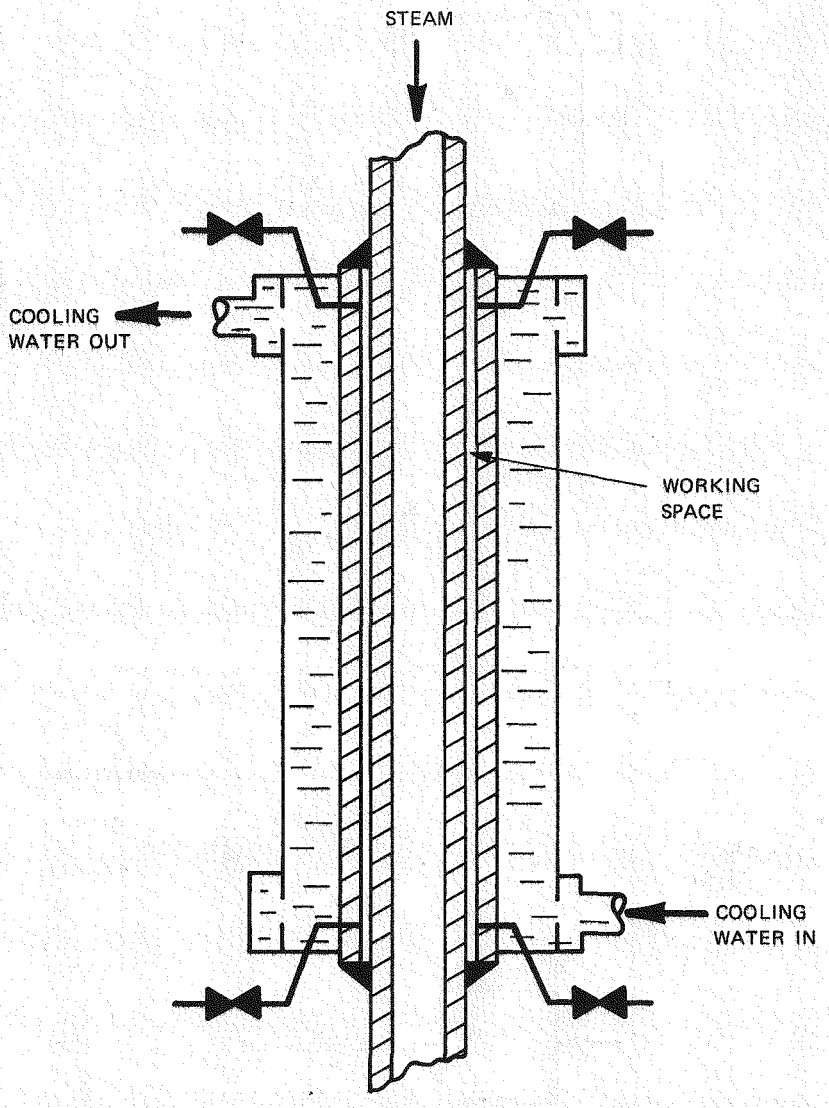

FIGURE 20 - Liquid thermal diffusion column.

efficiency of the system;[34] however, the transport profiles of the two cascades are far from ideal.

Purified degassed carbon disulfide at the cascade pressure of 17 atm is fed at a point one stage from the top of the first cascade. Reagent grade CS_2 is treated with mercury, dried over P_2O_5 and distilled in a high efficiency column under a helium atmosphere prior to transfer to the feed bottle. Pressure is maintained in the feed bottle by compressed helium acting through a mercury piston.

Carbon disulfide depleted in $C^{32}S^{34}S$ to 5.8% (2.8% ^{34}S) is removed from the top of the first cascade through a capillary leak at a rate of 35 g/day. Enriched product is removed from the bottom of the first cascade twice daily, five days a week, in batches of 3.4 g each. The first cascade product is preferentially enriched in the mixed molecule, $C^{32}S^{34}S$.

Cascade calculations and spot analyses show that the molecular composition departs significantly from an equilibrium distribution of isotopic substitutions. A typical calculated composition of this stream is given in Table 12.

In previously reported experimental work with CS_2,[35] it was determined that isotopic equilibration takes place rapidly in the gas phase at temperatures greater than 700°C. Accordingly, the product batches from the first cascade are passed through a quartz reactor at 800°C to effect a partial conversion of $C^{32}S^{34}S$ to $C^{32}S^{32}S$ and $C^{34}S^{34}S$. A calculated composition of the exchanged stream, assuming 80% conversion, is also given in Table 12.

The exchanged material, now containing an increased concentration of the desired material ($C^{34}S^{34}S$), is injected into second cascade at a point one stage from the top. As the batch is injected, it displaces a like amount of material depleted in $C^{34}S^{34}S$ from the top of the second cascade. The depleted material is returned to the first cascade at a point one stage from the bottom.

The present configuration of the liquid thermal diffusion system evolved from a number of cascade experiments with systems of fewer columns.[36] Dual cascade operation with an 11-column system was started on February 20, 1975. At that time, the apparatus was essentially the same as it is now; but the last column of the second stage had not been installed. The full 12-column system became operational on May 13, and the desired product concentration of 90% ^{34}S was reached on May 27. Product flow was started at 0.65 g/wk of CS_2 and was increased to 1.25 g/wk on June 2. Figure 21 is a plot of the concentration at the product point as a function of time.

The measured composition of a typical product sample is given in Table 12. These results, which are derived from a mass spectrometric scan of carbon disulfide, are based on assumptions which are required to resolve several mass interferences involving small but significant amounts of ^{13}C, ^{33}S, and ^{36}S. The ^{36}S concentration especially, may be in error by as much as 50% of the amount present. Future mass spectrometric work with samples burned in $^{16}O_2$ should eliminate ambiguities in the results.

Theoretical Calculations The computer program for calculating the transient behavior of multicomponent isotope separation cascades was modified to handle the two-cascade problem. In the program, the cascades are alternately stepped forward in time. A control subroutine sets up the feed and product streams associated with the intercascade flows, and a second routine simulates the exchange reactor.

Calculations were done for an 11-column system with 7 columns in the first cascade and 4 columns in the second and for a 12-column system with 5 columns in the second cascade. Carbon disulfide, for the purpose of the calculations, was assumed to be made up of the 10 most abundant molecular species out of the 20 possible combinations of carbon and sulfur isotopes. Column parameters assumed in the calculations are given in Table 11. The calculated ^{34}S concentrations at the bottom of the second cascade are plotted on Figure 21 with the experimental data. The calculated curve for the 12-column system was shifted in time to give the best agreement with experimental results.

Figure 19 represents the calculated conditions for the first point after 90% ^{34}S was reached. These calculations did not provide for a flow of product from the bottom of the second cascade. Note that the flow rate of the depleted stream from the top of the first cascade is somewhat lower than the experimental value.

Table 12

CARBON DISULFIDE COMPOSITIONS IN THE LIQUID THERMAL DIFFUSION SYSTEM

	Cascade I[a] Product (%)	Exchanged[a] Material (%)	Sulfur-34[b] Product (%)
^{12}C	97.88	97.88	95.2
^{13}C	2.12	2.12	4.8
^{32}S	64.18	64.18	3.9
^{33}S	2.35	2.35	1.1
^{34}S	33.36	33.36	91.0
^{36}S	0.106	0.106	3.9
$C^{32}S^{32}S$	31.63	39.28	0.026
$C^{32}S^{33}S$	3.88	3.21	0.053
$C^{32}S^{34}S$	61.00	46.44	4.6
$C^{33}S^{34}S$	0.82	1.49	2.2
$C^{34}S^{34}S$	2.45	9.37	85.2
$C^{32}S^{36}S$	0.20	0.15	3.0
$C^{34}S^{36}S$	0.0088	0.062	4.8

[a]From transient cascade calculation.

[b]Measured, June 4, 1975.

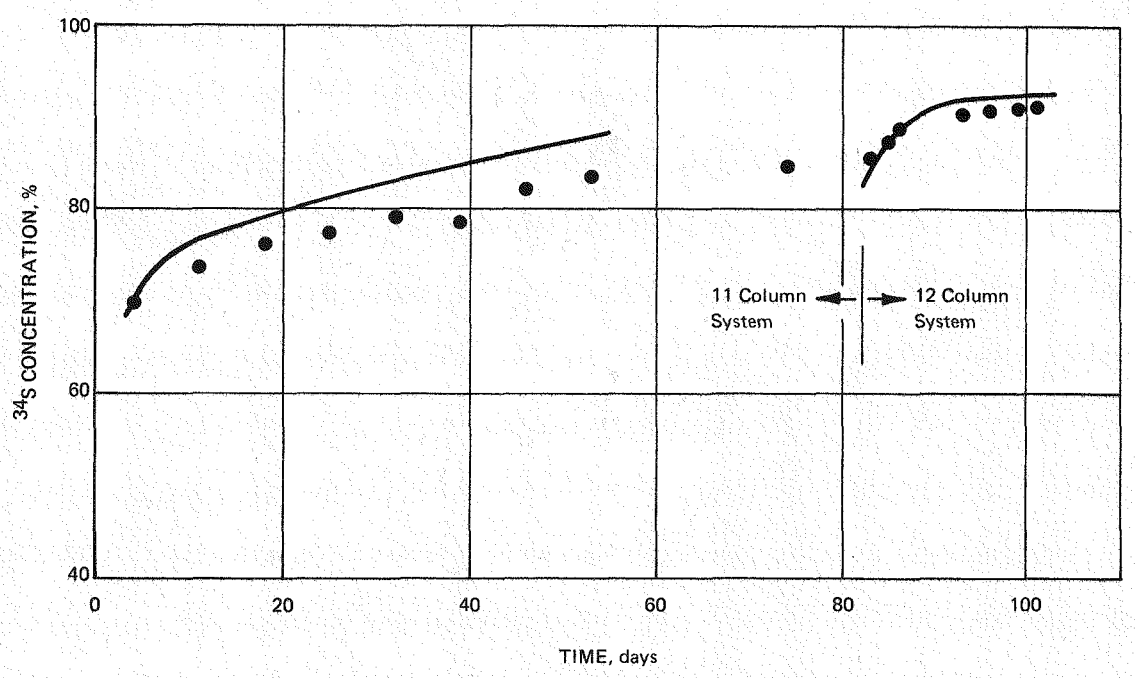

FIGURE 21 - Sulfur-34 separation in the liquid thermal diffusion system (the solid lines are calculated; zero time represents the start of dual cascade operation).

In order to get reasonable agreement with the observed distribution of ^{13}C in the experimental samples, it was necessary to use an effective mass difference of 0.67 between the ^{12}C and ^{13}C substituted molecules which suggests that the thermal diffusion factors in this system are influenced by parameters other than mass difference. A similar phenomenon was observed previously in work with the isotopically substituted benzene system.[37] *(W. M. Rutherford)*

MOLECULAR BEAM SCATTERING

Total scattering cross sections have been measured for the scattering of an argon beam off of krypton target particles (Ar-Kr) and the reverse scattering system of krypton off of argon target particles (Kr-Ar). These measurements were made with a controlled target cell temperature of 300 K and beam source temperatures of 180 K and 300 K. A summary of the reduced data is given in Table 13 along with the calculated effective total scattering cross section Q_e. The quantity Q_e (Av) is the weighted average cross section. The weighting is determined by the deviation of the data from the least square fitted curve of the beam attenuation ln I/I_o vs the target cell gas density, n, for the respective experimental run. The uncertainties shown relate to this experimental data spread. From the table, it can be seen that the spread is quite small (1.0%-4.8%) and reproducible. The calculation methods used have been previously described.[38]

The two comparison experiments, TOT 23 and TOT 24, were run at slightly different relative velocities. This should account for about 1% disagreement between the final relative velocity cross sections. Final evaluation of the average relative velocity cross sections has not been completed. Accurate determination of the velocity distribution functions for the target gas, detector, and beam are necessary for the calculation of the proper average velocity correction factors. These distributions are known for the target gas and detector but not for the nozzle beam. The precise velocity distribution of a supersonic nozzle beam cannot be easily determined from theoretical models because of the influence of the difficult-to-measure parametric effects such as nozzle jet density, Mach number, temperature in the jet, and boundary layer characteristics at the skimmer. The addition of a quadrupole detector will provide a time-of-flight measurement when used with the beam chopper. A direct experimental determination of the beam velocity distribution should then be possible.

A new capillary leak has been added to the target gas cell feed system. The new leak uses a larger diameter capillary with more length to achieve approximately the same calibrated flow regime. Because of its small diameter, the old capillary became partially plugged; and thus, the calibration was destroyed. The new system has operated quite well, showing no tendency to plug. It was necessary to recalibrate the new system for each gas to be used. This procedure was described in an earlier report.[39]

The quadrupole molecular beam detector, which has been previously described, has been undergoing tests.[38] With the system described, a modulated molecular beam signal was detected by the phase sensitive detector. However, the phase-locked ac signal, which was detected, only dropped by 10% when the beam shutter was closed, indicating that the ac signal from the chopper motor was overriding the beam signal. This signal was traced to a capacitance/inductance field coupling between the chopper wheel and the quadrupole. A new, tuning fork type beam chopper (manufactured by Bulova) was mounted in the system. This new chopper system eliminates the extraneous phase-locked ac signal. Sensitivity measurements have been made using neon-20 as the beam gas. The beam density at the ionizer is calculated to be 1.6×10^{10} P_s particles/cm^3, where P_s is the pressure in the source measured in torr. When P_s is 0.1 torr, the particle density at the ionizer is 1.6×10^9 particles/cm^3. The ac voltage signal measured by the phase sensitive detector that corresponds to this density can be maximized at around 100 μV. Further tests are being conducted to ascertain the noise level of the detector system compared with the beam signal that can be detected.

The historical water corrosion problem has hopefully been remedied by the installation of a completely new recirculating pumped system. The water supply will now be received from the thermal diffusion systems cooling tower, filtered, pumped to the necessary pressure required to produce adequate flow for the beam chamber system, and returned to the tower for cooling. The new system has just been completed and is now in its trial stages. This should eliminate the age-old water damage that has plagued the beam project from its beginning. *(R. W. York and R. E. Miers)*

Table 13

SUMMARY - ARGON-KRYPTON AND KRYPTON-ARGON[a]
TOTAL CROSS SECTIONS

Scattered Pair	Experiment No.	Source Temperature (K)	V_b (cm/sec)	V_r (cm/sec)	Q_e A^2	$Q_{e(Av)}$ Weighted	UNC. (estimated %)
Ar-Kr	TOT-22A	300	5.59×10^4	6.23×10^4	342.8	363.8	+4.8
	TOT-22B	300	5.59×10^4	6.23×10^4	368.1		-2.3
Ar-Kr	TOT-24A	180	4.33×10^4	4.99×10^4	421.7	426.5	+1.1
	TOT-24B	180	4.33×10^4	4.99×10^4	430.6		-1.0
Kr-Ar	TOT-23A	180	2.99×10^4	5.13×10^4	347.5	353.8	+1.8
	TOT-23B	180	2.99×10^4	5.13×10^4	359.9		-1.7

[a] Target temperature = 300 K; most probable target velocity $V_t = 2.44 \times 10^4$ cm/sec (Kr) and $V_t = 3.53 \times 10^4$ cm/sec (Ar); V_b = most probable beam velocity; $y = V_b/V_t$.

TRANSPORT PROPERTIES

Thermal Diffusion Factor for ^{3}He-^{4}He Experimental results for the thermal diffusion factor, α_T, of an equimolar mixture of ^{3}He-^{4}He below 10 K were given in a previous report,[40] along with theoretical predictions for α_T using five proposed intermolecular potentials. Quantum mechanical calculations for α_T have been performed for two additional potentials proposed in the literature: 1) the Hybrid Morse-V_{DD} (MDD-2) potential by Bruch and McGee[41] with new parameters, and 2) a potential from molecular beam scattering results by Farrar and Lee[42] (FL). These results are shown in Figure 22.

Five of the potentials demonstrate similar behavior and lie in a narrow band with maxima at approximately 2 K. MDD-3, which is a "screened" two-body potential for liquid helium, rises steeply to values of 0.185 and 0.292 at 2.5 and 1.0 K, respectively, in a fashion unlike that of the other potentials. Sposito[43] has noted that there does not appear to be any comparison heretofore of the effects of the "screening" upon the bare two-body potential which, besides predicting α_T too high at low temperatures, is somewhat low at elevated temperatures. Sposito, however, demonstrates that MDD is a correct functional form for an effective two-body potential for liquid helium while LJ is not. ONLY MDD-1 approximates the behavior of the experimental data, which show an ill-defined maximum around 3 or 4 K then drop off rapidly below 3 K. Farrar and Lee performed scattering at a collision energy corresponding to approximately 55 K, which perhaps is not low enough to provide a proper representation of the potential in the region of interest here.

Bruch and McGee have tested for an overall fit of both MDD-1[44] and MDD-2 to dilute helium gas data from 1 to 2000 K and find MDD-2 to be superior overall. Deviations remain, however, which cannot be removed by parameter adjustment without causing greater problems in another region of the fit. MDD-1 is unique among the potentials investigated in that it has the deepest well suggesting a large area in the attractive region which Sposito has considerably diminished by adjusting the well depth and multipole parameters to fit the liquid properties. On the basis of the present available information we would, therefore, recommend a "bare" two-body helium potential of the MDD functional form with essentially the same area in the attractive region as MDD-1, but with a slightly shallower and broader well.

Thermal Diffusion Factor for Xenon Experimental and theoretical thermal diffusion factors for isotopic xenon were reported previously in this series.[48] The experimental trannschaukel data, along with the thermal column data of Rutherford,[49] were fitted to a function of the form:

$$\alpha_T = A + \beta/T^{1/2} + C/T^2,$$

with A = 0.041520, β = -0.757498, and C = 559.951 by the method of least squares. The average percent deviation of the fit was 3.8%, well within the experimental uncertainty. Of the potentials examined in the previous report,[48] that proposed by Parson-Siska-Lee[50] (with parameters by Lee[51] for xenon) gave the best overall fit. Recently, Barker[52] et al. have published a potential that was fitted to a wide variety of xenon properties including solid-state, dilute gas transport, and molecular beam scattering data, to name

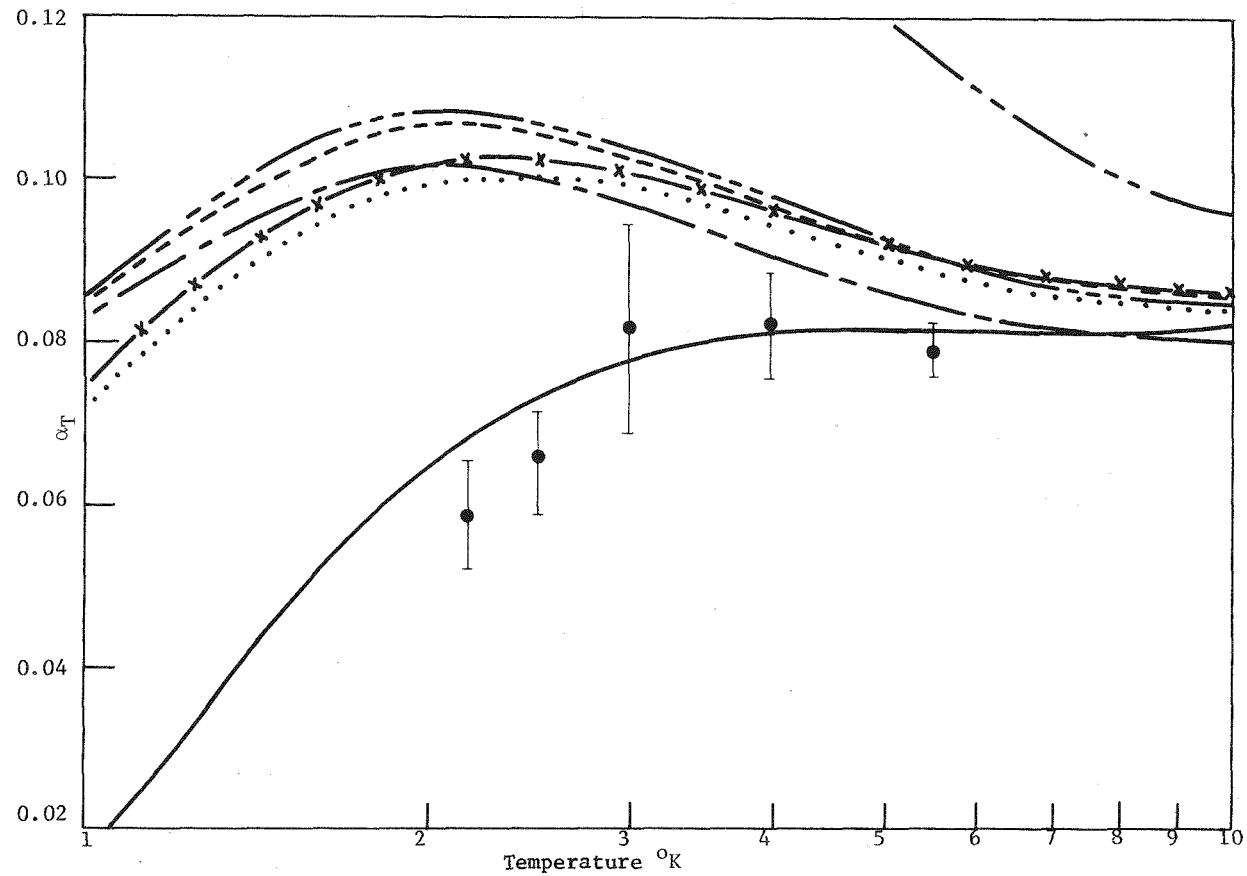

FIGURE 22 - α_T for an equimolar ^3He-^4He mixture. The solid circles are the previously reported experimental data. The theoretical curves are: ——, MDD-1;[44] —x—, MDD-2;[41] —--, MDD-3;[43] ---, Beck;[45] ....., FL;[42] —-—, (exp-6);[46] and —---, LJ;[47]

a few. It appeared likely that this potential, with its large number of adjustable parameters (17) and proven fit to many properties, should be accurate. Classical collision integrals were calculated using the xenon parameters given by Barker et al. and theoretical values of $(\alpha_T)_3$ evaluated therefrom. The deviation plot of this and the Parson-Siska-Lee potential are shown in Figure 23. The base line (zero) in the figure represents the least squares fit to the data. The dotted curves represent the estimated experimental uncertainty envelope. As shown by the position of the triangles, the PSL potential falls outside the estimated uncertainty envelope at low temperatures but is quite acceptable above 300 K. On the other hand, the new potential by Barker et al. is entirely within the uncertainty envelope and in complete agreement with the thermal diffusion measurements. *(W. L. Taylor)*

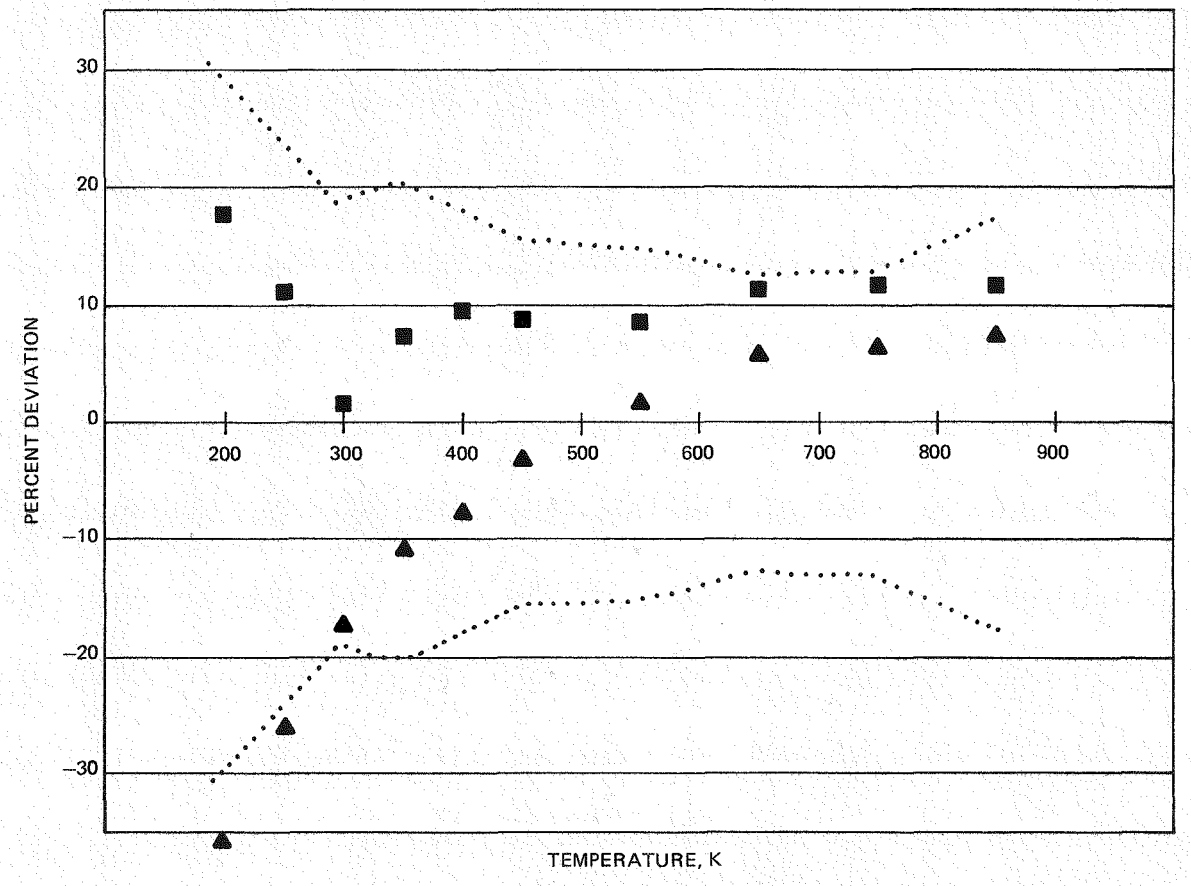

FIGURE 23 - Percent deviation plot of the theoretical thermal diffusion factor, $[\alpha_T]_3$, for ^{124}Xe-^{136}Xe from the least square fit to the experimental data (the dotted lines represent the envelope of estimated uncertainty for the experimental data; Δ, the Parson-Siska-Lee[50,51] potential; and □, the Barker et al.[52] potential).

References

1. Mound Laboratory Activities for the Division of Physical Research: July-December 1974, MLM-2198 (April 10, 1975), pp. 11-14.
2. A. J. Maeland, J. Phys. Chem., 68, 2197 (1964).
3. R. M. Cotts, Ber. Bunsenges. Physk. Chem., 76, 760 (1972).
4. B. Stalinski, Ber. Bunsenges. Physk. Chem., 76, 724 (1972).
5. H. Asano and M. Hirabayaski, Phys. Stat. Sol. (a), 16, 69 (1973).
6. R. R. Arons, H. G. Bohn, and H. Lutgemeier, J. Phys. Chem. Solids, 35, 207 (1974).
7. B. Pedersen, T. Krogdahl, and O. E. Stokkeland, J. Chem. Phys., 42, 72 (1965).
8. D. Rohy and R. M. Cotts, Phys. Rev., B1, 2070 (1970).
9. H. T. Weaver, Phys. Rev., B6, 2544 (1972).
10. C. Korn and Zamier, J. Phys. Chem. Solids, 31, 489 (1969).
11. H. T. Weaver, Phys. Letters, 35A, 417 (1971).
12. H. Lutgemeier, R. R. Arons, and H. G. Bohn, J. Mag. Resonance, 8, 74 (1972).
13. J. J. Reilly and R. H. Wiswall, Inorg. Chem., 13, 218 (1974).
14. J. Federer, Purification of Iridium by an Oxidation-Dissolution Process, ORNL-TM-4665 (October 1974), 26 pp.
15. C. Duval, Inorganic Gravimetric Analysis (second edition), Elsevier Publishing Co., N. Y., 1963, p. 589.
16. Mound Laboratory Activities for the Division of Physical Research: January-June 1974, MLM-2168 (August 30, 1974), p. 31.
17. Mound Laboratory Activities for the Division of Physical Research: July-December 1973, MLM-2118 (February 28, 1974), p. 32.
18. G. L. Silver in Mound Laboratory Activities for the Division of Physical Research: July-December 1974, MLM-2198 (April 10, 1975), pp. 38-42.
19. S. O. Zimmerman, Bull. Mathematical Biophysics, 28, 433 (1966).
20. J. B. Best and J. Z. Hearon in Mineral Metabolism, C. L. Comar and F. Bronner (eds.), Vol. 1A, Academic Press, New York, 1960, pp. 12-60.
21. C. Y. C. Pak and F. C. Bartter, Biochimica et Biophysica Acta, 141, 401 (1967).
22. C. Y. C. Pak and F. C. Bartter, op. cit., 141, 410 (1967).
23. W. V. Loebenstein, J. Colloid and Interfacial Science, 36(2), 234 (1971).
24. M. M. Golutvina, L. S. Semochkina, N. N. Kononykina, and V. M. Ezhova, Radiokhimiya, 15(4), 636 (1973).

25. W. F. Schmid, M. A. Aia, and R. W. Mooney, J. Inorg. Nucl. Chem., 28, 1325 (1966).

26. W. V. Loebenstein, J. Res. Nat. Bur. Stds., 66A(6), 503 (1962).

27. M. C. Bennett and J. C. Abram, J. Colloid and Interfacial Science, 23, 513 (1967).

28. G. L. Silver, Radiochem. Radioanal. Letters, 7, 213 (1971).

29. G. L. Silver, J. Inorg. Nucl. Chem., 35, 1369 (1973).

30. Mound Laboratory Activities for the Division of Physical Research: July-December 1972, MLM-2013 (February 14, 1973), pp. 56-59.

31. Mound Laboratory Activities for the Division of Physical Research: July-December 1974, MLM-2198 (April 10, 1975), p. 45.

32. G. L. Silver, Anal. Chem., 41:3, 548 (1969).

33. R. C. Jones and W. H. Furry, Rev. Mod. Phys., 18, 151 (1946).

34. K. Cohen, The Theory of Isotope Separation as Applied to the Large-Scale Production of U-235, McGraw-Hill, New York, 1951.

35. Mound Laboratory Activities for the Division of Physical Research: July-December 1974, MLM-2198 (April 10, 1975), p. 46.

36. Mound Laboratory Activities for the Division of Physical Research: January-June 1974, MLM-2168 (August 30, 1974), p. 22.

37. W. M. Rutherford, J. Chem. Phys., 59, 6061 (1974).

38. Mound Laboratory Activities for the Division of Physical Research: July-December 1974, MLM-2198 (April 10, 1975), pp. 52-57.

39. Stable Gaseous Isotope Separation and Purification: April-June 1972, MLM-1943 (August 18, 1972), pp. 11-13.

40. Mound Laboratory Activities for the Division of Physical Research: January-June 1974, MLM-2168 (August 30, 1974).

41. L. W. Bruch and I. J. McGee, J. Chem. Phys., 52, 5884 (1970).

42. J. M. Farrar and Y. T. Lee, J. Chem. Phys., 56, 5801 (1972).

43. G. Sposito, J. Low Temp. Phys., 3, 491 (1970).

44. L. W. Bruch and I. J. McGee, J. Chem. Phys., 46, 2959 (1967).

45. D. E. Beck, Mol. Phys., 14, 311 (1968); 15, 332 (1968); J. Chem. Phys., 50, 541 (1969).

46. J. E. Kilpatrick, W. E. Keller, and E. F. Hammel, Phys. Rev., 97, 9 (1955).

47. J. deBoer and A. Michels, Physica, 5, 945 (1938).

48. Mound Laboratory Activities for the Division of Physical Research: July-December 1973, MLM-2118 (February 28, 1974).

49. W. M. Rutherford, J. Chem. Phys., 58, 1613 (1973).

50. J. M. Parson, P. E. Siska, and Y. T. Lee, J. Chem. Phys., 56, 1511 (1972).

51. Y. T. Lee, Proc. of the 1973 Conf. on Gas Kinetics, 27 (1973).

52. J. A. Barker, R. O. Watts, J. K. Lee, T. P. Schafer, and Y. T. Lee, J. Chem. Phys., 61, 3081 (1974).

DISTRIBUTION

External

TID-4500, UC-4 and 22 (164)

W. J. Haubach, Molecular and Geo-Sciences Br.,
Div. of Physical Research, ERDA

Consultants

C. F. Curtiss,
University of Wisconsin
C. F. Eck
Miamisburg, Ohio
D. F. Griffing
Miami University (Ohio)
R. E. Miers
Ft. Wayne, Indiana
G. W. Powell
Ohio State University
A. Shapiro
University of Cincinnati
H. F. Swift
University of Dayton Research Institute
D. White
University of Pennsylvania
H. W. Mattson
Monsanto Company

Internal

V. L. Avona
W. T. Cave
R. J. DeSando
B. E. Jepson
L. V. Jones
E. Michaels
W. J. Roos
W. M. Rutherford
R. A. Schwind
G. L. Silver
W. L. Taylor
R. E. Vallee
J. G. Villars
R. L. Wainwright
R. M. Watrous

Document Control
Library (15)
Publications